A macrocyclic ‘Co^0’ complex: the relevance of ligand non-innocence to reactivity†

Manuel Kaspar,[a] Philipp J. Altmann,[a] Alexander Pöthig,[a] Stephen Sproules,[b] Corinna R. Hess*[a]

[a] Department of Chemistry and Catalysis Research Center, Technische Universität München, Lichtenbergstrasse 4, D-85747, Garching (Germany). Email: corinna.hess@ch.tum.de

[b] WestCHEM, School of Chemistry, University of Glasgow, Glasgow G12 8QQ (UK)

†Electronic Supplementary Information (ESI) available: Experimental details for the synthesis of **1** and **3**, spectroscopic data and CIFs. See DOI: 10.1039/x0xx00000x

We present a formally zero-valent compound, [Co(Mabiq)Na(OEt$_2$)]$_2$ (1). The complex was characterized by crystallographic, spectroscopic and DFT computational methods. The electronic structure is described as a Co^{II}–(ligand-biradical). Compound 1 is reactive toward proton sources; Co^{I} or Co^{II} products result, depending on the source of protons used. The redox non-innocence of the Mabiq ligand, which accepts both protons and electrons, has important ramifications for reactivity.

The advancement of solar fuel technologies is vital for the global progression toward renewable energy sources.[1] The development of robust and inexpensive catalysts for the conversion of protons or CO_2 into energy-rich chemicals is integral to these efforts.[2-4] Among the suitable noble-metal free complexes, molecular cobalt compounds have demonstrated significant promise as both electro- and photocatalysts for both reactions.[5-8] These compounds encompass a diverse array based on unsaturated N_4-macrocyclic, pyridyldiimine, polypyridine, triphos and dithiolene ligands.[9-17] The reactivity of the complexes hinges on the formation of low-valent forms: typically a Co^{I} species is invoked in catalytic cycles for H_2 evolution.[6,7] However, in several cases, generation of the more nucleophilic Co^{0} species is required for reactivity of the complexes.[6,7,9,15,17-19] A few Co^{I} compounds have been isolated among known catalysts.[9,14,20] However, the Co^{0} species remains elusive among these systems, its properties gleaned only on the basis of indirect and theoretical evidence.[21,22] The electronic structure of the zero-valent intermediate is of further intrigue, as this reduced form might in actuality possess substantial ligand radical character. A true Co^{0} compound may well be supported by triphos and macrocyclic aminopyridine ligands.[9,14] However, the alternative Co^{I}L$^{\bullet}$ description is recognized as a more accurate depiction of the doubly-reduced species among compounds containing porphyrin and diimine-based ligands, for example.[6,18,19,23] This ligand non-innocence may have important consequences for proton coupled electron transfer processes associated with both H_2 evolution and CO_2 activation.[12,18,19,23-25] The Co^{0} complex is, therefore, a missing yet pivotal piece of mechanistic puzzles. Furthermore, the

reactivity of this supernucleophile remains unexplored. Insight into the electronic structure of the doubly reduced species will guide our understanding of its chemistry.

Toward this end, we have now isolated a doubly reduced, *formally* zero-valent compound, $[Co(Mabiq)Na(OEt_2)]_2$ (**1**, Scheme 1), based on our N_4-macrocyclic Mabiq ligand. Compound **1** completes the electron transfer series of our Co-Mabiq complexes, which already included the formally monovalent Co(Mabiq) (**2**),[26] and now encompasses the full complement of formal oxidation states ($0 \rightarrow +3$) invoked in the catalytic cycles of the HER and CO_2 reduction. The characterization of **1** by crystallographic, spectroscopic and DFT computational methods is described herein. Preliminary studies examining the reactivity of **1** toward proton source also are presented. The results already highlight ramifications of proton and electron storage by the redox-active Mabiq ligand for reactivity.

In association with the present work, a new form of the cobaltous-Mabiq complex, $[Co(Mabiq)(THF)](PF_6)$ (**3**), also was synthesized. The molecular structure (Figure S1) resembles that of the previously isolated Co(Mabiq)Cl,[26] except a solvent molecule occupies the axial position in lieu of the chloride ligand. Compound **3** was deemed more suitable for comparison of products obtained in the reaction of **1**. The electronic spectrum of **3** closely resembles that of Co(Mabiq)Cl, with minor shifts in the absorption bands. The EPR spectrum recorded at room temperature is consistent with a low-spin Co^{II} center (Figure 1). The 8-line pattern from coupling with the ^{59}Co $I = {}^7/_2$ (100%) isotope is larger than for [Co(Mabiq)Cl].[26]

The title Co^0 compound was obtained upon treatment of Co(Mabiq) with one equivalent of Na in THF, yielding the dark red **1**. The compound is dimeric in the solid state (Figure 2); the two bipyrimidine (bpm) units are within π-stacking distance (3.47 Å). A sodium ion coordinates the external diimine group of each monomeric unit, and further promotes association of the two macrocycles. The short contacts between the alkali metal situated in the bpm moiety of one

molecule, and the N-atom of the neighboring bpm (Na–N1a = 2.676(3) Å) betrays significant electron density on the biquinazolines.[27] The shortened C–C and longer C–N bond distances of the bpm diimine moiety, in comparison to those of **2** and **3** (Table S2), allude to ligand-centered reduction.

The electronic spectrum of **1** (Figure S5) shares several features with that of **2**, notably intense bands centered at 525 nm, along with NIR absorptions, none of which appear in the spectrum of the cobaltous **3**. However, compound **1** exhibits a unique, pronounced transition at 442 nm, as well as shoulders (ca. 600 and 650 nm) to the 532 nm absorption. A transition at 429 nm also features in the spectrum of **3**, which otherwise is distinguished by a series of bands in the visible region (550 – 700 nm). Compound **1** most likely exists as a monomer in solution; the π- and intermolecular Na-N interactions that govern association of the macrocycles in the solid state are unlikely to persist in solvent. The EPR spectrum of **1** is diagnostic of a ligand-centered unpaired spin with a featureless line, with g_{iso} = 2.0029 (Figures 1 and S25). A satisfactory fit included a miniscule $A\{^{59}Co\}$ coupling of 1.05×10^{-4} cm^{-1} commensurate with the <0.5% Co content of the SOMO (*vide infra*). The addition of 15-Crown-5 to a solution of **1** had no effect on the EPR spectrum.

The electronic structure of **2** was previously described by $Co^{I}(Mabiq^{-}) \leftrightarrow Co^{II}(Mabiq^{2-\bullet})$ resonance forms on the basis of density functional (DFT) calculations.[26] $[Co^{I}(Mabiq^{2-\bullet})]^{-}$ and $[Co^{II}(Mabiq^{3-})]^{-}$, containing the one- or two-electron reduced macrocycle, likewise offer alternate formulations of the formally zero-valent complex. DFT (B3LYP) calculations on the monomeric form of the compound, $[Co(Mabiq)Na(OEt_2)]$, yielded an open-shell solution supporting the $[Co^{II}(Mabiq^{3-})]^{-}$ description of **1**. The DFT-derived spin-density map (Figure 3) depicts two electrons of alpha-spin on the macrocycle, and one electron of beta-spin on the metal ion. Three doubly occupied metal-based orbitals can be identified by inspection of the

DFT-derived molecular orbitals (Figure S4) and the Loewdin population analysis. The unpaired electron on the cobalt ion resides in the *xz* orbital. The corresponding ligand-centered radical of opposite spin occupies a diketiminate π* orbital, as seen in the neutral series of compounds: $Co^{II}(Mabiq^{2-\bullet})$, $Fe^{II}(Mabiq^{2-\bullet})$ and $Zn^{II}(Mabiq^{2-\bullet})$.[26,28] However, the final SOMO in the MO depiction of **1** represents a bpm-based π* orbital. Although the first ligand-centered reduction consistently involves the diketiminate, the bpm clearly also is redox-active. The DFT results, denoting antiferromagnetic coupling between an $S = {}^1/_2$ Co^{II} ion and an $S = 1$ Mabiq di-radical, are consistent with the EPR data.

Compound **1** is indeed reactive toward proton sources (product spectra, Figure S6). A solution of **1** in THF immediately changes color from red to purple, upon addition of benzoic acid (5 equiv.). The product absorption spectrum indicates the formation of a Co^{I} species. The reaction of **1** with one equiv. *p*CA also produces a Co^{I} species; the product spectrum is again similar, but not identical, to that of **2**. At higher acid concentrations, further conversion to a Co^{II}-containing compound occurs. The product spectrum typifies a Co^{II} species, with the characteristic absorption features in the visible region, but does not precisely match that of **3**. For comparison, the addition of *p*CA to a solution of **2** likewise yields a Co^{II} compound; in this case, the product spectrum is superimposable with that of **3** (Figure S6), suggesting clean conversion to the oxidized form. The monovalent compound does not react with benzoic acid; as expected, the doubly-reduced **1** is more nucleophilic than **2**, such that it reacts even with weak acids.The products of the **1**/acid reaction mixtures were further analyzed by ^{1}H NMR spectroscopy (Figure S7 – S15). Two diamagnetic products are produced in the **1**/benzoic acid and **1**/*p*CA reactions (5 equiv. benzoic acid; 1 equiv. *p*CA), which could be separated by chromatography. The primary reaction product corresponds to **2**, as evidenced by the NMR spectrum (Figure 4, bottom). The NMR spectrum of the second product (30 – 50%) exhibits eleven proton

resonances in the aromatic region, denoting desymmetrization of the macrocyclic ligand (Figure 4, top). Three singlets are present at 7.47, 7.30 and 6.52 ppm. The resonance at 7.30 ppm can be assigned to the diketiminate proton. The additional two signals at 6.52 and 7.47 ppm correspond to protons situated at bpm N and C atoms, respectively, based on the COSY, HSQC and HMBC spectra (Figure S13 – S15).

The one-electron oxidized, diamagnetic [Co(MabiqH$_2$)] (**[2-H$_2$]**), containing a doubly protonated Mabiq ligand describes the second product in the reaction of **1** with acid. The molecular structure of **[2-H$_2$]** (Figure S29) offers further evidence that the bpm unit is altered. The negatively charged diimine component of **1** readily takes up the acidic protons. No evidence of H_2 was observed by NMR for any of the **1**/acid reactions. We thus propose that the formation of **[2-H$_2$]** could proceed according to Scheme 2.

The initial protonation of **1** leads to the formation of a [Co^{II}(MabiqH$_2$)]$^-$ species. Subsequent intermolecular electron transfer involving a second molecule of **1** yields a mixture of **2** and **[2-H$_2$]**, as observed by NMR.

We note that ligand protonation does not generally ensue under acidic conditions. Mass spectrometry data (Figures S16 – S23) of **3**/acid mixtures shows only a peak of *m/*z = 600 ([M]$^+$), corresponding to the parent complex. Ligand protonation also does not occur upon addition of benzoic acid to a solution of **2**, whereas with *p*CA, an additional peak of *m/z* = 602 ([M+2]$^+$) is observed, as for the **1**/acid reactions. Radical character in **2** may likewise render the macrocycle susceptible to modification by strong acids.

The reactivity of **1** parallels the behavior predicted in computational studies for low-valent porphyrin compounds. The generation of a phlorin intermediate in the mechanism of H_2 evolution by 'Co^0'-porphyrins is thermodynamically favored over metal-hydride formation.[23] The preferred ligand protonation is a consequence of porphyrin radical character in the zero-

valent form. Doubly protonated porphyrin intermediates are generated in the HER by hangman porphyrins and require further reduction to effect H_2 release.[23,29]

Compound **[2-H$_2$]** does not appear to release H_2. No change was observed in the NMR spectrum of **[2-H$_2$]**, even upon heating of a sample to 50 °C. **[2-H$_2$]** also does not react appreciably with proton sources. Only minor changes in the absorption spectrum are observed upon addition of *p*CA (up to 15 equiv., THF; Figure S30). **[2-H$_2$]** also does not react with TEMPO-H.

Interestingly, the CV of **[2-H$_2$]** shows that the values for the $Co^{III/II}$ and $Co^{II/I}$ redox potentials are similar to those of **3** (Figure S31). Protonation of the bpm moiety appears to have a negligible influence on the metal center. Furthermore, the formal $Co^{II/I}$ couple may involve reduction of the diketiminate unit, as observed for **3**. This group is situated furthest away from the ligand protonation site. The $Co^{I/0}$ couple of the modified Mabiq complex exhibits the largest shift, by -100 mV, consistent with reduction of the bpm unit upon addition of the second electron. The electronic structure of **[2-H$_2$]** is analogous to that of **2**: the DFT-derived (B3LYP, BS1,1) spin density plot (Figure S32) again depicts the radical character of the ligand, with electron density localized on the diketiminate moiety. The differing reactivity of **2** and **[2-H$_2$]** toward proton sources is thus surprising. The reactivity of these one-electron reduced forms remains to be examined in detail.

The current work, focusing on the properties and reactivity of the formally zero-valent **1**, highlights important lessons for the use of redox active ligands in proton coupled electron transfer processes. The generation of zero-valent compounds is thought to be necessary for the reduction of weak acids by numerous HER catalysts. Since reduction of our cobaltous compound is clearly ligand-centered, the macrocycle rather than the metal takes up added protons. Consequently, our doubly reduced Co^{II}–(ligand-biradical) complex appears to be

unviable for the hydrogen evolution reaction. The 'zero-valent' and $M^{I}L^{\bullet}$ intermediates cited among other molecular systems should be examined in greater detail. A genuine Co^{0} intermediate likely will react with protons in a different manner to our complex, via a metal-hydride species that could effectively release H_2. However, among the many cobalt systems containing redox-active ligands, the ligand may likewise compete with the metal center for both electrons and protons. A greater understanding of the scenarios under which such ligand frameworks inhibit or support reactivity will be important for HER catalyst design. Regardless, the incorporation of non-innocent ligands in coordination complexes offers a powerful tool for other redox reactions,[30] and may in fact favor CO_2 redution.[19] The broader reactivity of the doubly-reduced **1** toward other substrates, including CO_2, will be explored in future work.

The authors thank Prof. Klaus Köhler for the use of his EPR spectrometer, and Dr. Carmen Haeßner for technical assistance. MK and PA thank the TUM Graduate School for financial support.

Notes and References

1. N. S. Lewis and D. G. Nocera, *Proc. Natl. Acad. Sci*, 2006, **103**, 15729-15735.
2. J. R. McKone, N. S. Lewis and H. B. Gray, *Chem. Mater.*, 2014, **26**, 407-414.
3. S. Berardi, S. Drouet, L. Francàs, C. Gimbert-Suriñach, M. Guttentag, C. Richmond, T. Stoll and A. Llobet, *Chem. Soc. Rev.*, 2014, **43**, 7501-7519.
4. M. Rakowski DuBois and D. L. DuBois, *Acc. Chem. Res.*, 2009, **42**, 1974-1982.
5. N. Kaeffer, M. Chavarot-Kerlidou and V. Artero, *Acc. Chem. Res.*, 2015, **48**, 1286-1295.
6. N. Queyriaux, R. T. Jane, J. Massin, V. Artero and M. Chavarot-Kerlidou, *Coord. Chem. Rev.*, 2015, **304-305**, 3-19.

7. J. R. McKone, S. C. Marinescu, B. S. Brunschwig, J. R. Winkler and H. B. Gray, *Chem. Sci.*, 2014, **5**, 865-878.

8. J. Bonin, A. Maurin and M. Robert, *Coord. Chem. Rev.*, 2017, **334**, 184-198.

9. S. C. Marinescu, J. R. Winkler and H. B. Gray, *Proc. Natl. Acad. Sci. U.S.A.*, 2012, **109**, 15127-15131.

10. V. Artero and M. Fontecave, *Chem. Soc. Rev.*, 2013, **42**, 2338-2356.

11. C. Costentin, H. Dridi and J.-M. Savéant, *J. Am. Chem. Soc.*, 2014, **136**, 13727-13734.

12. B. H. Solis and S. Hammes-Schiffer, *Inorg. Chem.*, 2014, **53**, 6427-6443.

13. J. L. Dempsey, J. R. Winkler and H. B. Gray, *J. Am. Chem. Soc.*, 2010, **132**, 1060-1065.

14. A. Chapovetsky, T. H. Do, R. Haiges, M. K. Takase and S. C. Marinescu, *J. Am. Chem. Soc.*, 2016, **138**, 5765-5768.

15. Z. Guo, S. Cheng, C. Cometto, E. Anxolabéhère-Mallart, S.-M.-. Ng, C.-C. Ko, G. Liu, L. Chen, M. Robert and T.-C.-. Lau, *J. Am. Chem. Soc.*, 2016, **138**, 9413-9416.

16. W. R. McNamara, Z. Han, P. J. Alperin, W. J. Brennessel, P. L. Holland and R. Eisenberg, *J. Am. Chem. Soc.*, 2011, **133**, 15368-15371.

17. C. H. Lee, D. K. Dogutan and D. G. Nocera, *J. Am. Chem. Soc.*, 2011, **133**, 8775-8777.

18. L. Tong, A. Kopecky, R. Zong, K. J. Gagnon, M. S. G. Ahlquist and R. P. Thummel, *Inorg. Chem.*, 2015, **54**, 7873-7884.

19. D. C. Lacy, C. C. L. McCrory and J. C. Peters, *Inorg. Chem.*, 2014, **53**, 4980-4988.

20. X. Hu, B. S. Brunschwig and J. C. Peters, *J. Am. Chem. Soc.*, 2007, **129**, 8988.

21. S. Ciurli, S. Gambarotta, C. Floriani, A. Chiesi- Villa and C. Guastini, *Angew. Chem. Int. Ed.*, 1986, **25**, 553-554.

22. A search of the CCDC (July 2016) revealed only a Co(0)-tetraphenylporphyrin (TPP) structure (see Ref. 17). The reactivity of the complex was not examined.

23. B. H. Solis, A. G. Maher, T. Honda, D. C. Powers, D. G. Nocera and S. Hammes-Schiffer, *ACS Catal.*, 2014, **4**, 4516-4526.

24. L. M. A. Quintana, S. I. Johnson, S. L. Corona, W. Villatoro, W. A. Goddard, M. K. Takase, D. G. VanderVelde, J. R. Winkler, H. B. Gray and J. D. Blakemore, *Proc. Natl. Acad. Sci. U.S.A.*, 2016, **113**, 6409-6414.

25. R. M. Bullock and M. L. Helm, *Acc. Chem. Res.*, 2015, **48**, 2017-2026.

26. E. V. Puttock, P. Banerjee, M. Kaspar, L. Drennan, D. S. Yufit, E. Bill, S. Sproules and C. R. Hess, *Inorg. Chem.*, 2015, **54**, 5864-5873.

27. $[Na(THF)_3]^+$ ions were also present in the molecular structure of the Co^0-TPP complex (Ref. 17), situated above and below the porphyrin; the reported Na-N(TPP) bond distances (2.766(5); 2.757(5) Å) are longer than the analogous Na-N(2a) bond distances of **1**.

28. P. Banerjee, A. Company, T. Weyhermüller, E. Bill and C. R. Hess, *Inorg. Chem.*, 2009, **48**, 2944-2955.

29. B. H. Solis, A. G. Maher, D. K. Dogutan, D. G. Nocera and S. Hammes-Schiffer, *Proc. Natl. Acad. Sci. U.S.A.*, 2016, DOI: 10.1073/pnas.1521834112, 485-492.

30. P. J. Chirik and K. Wieghardt, *Science*, 2010, **327**, 794.

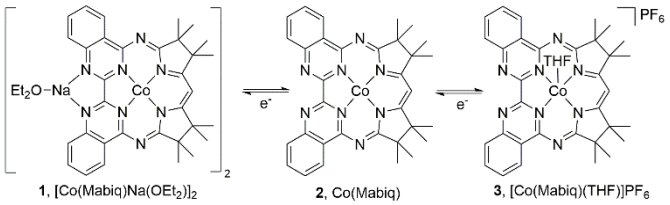

Scheme 1 Electron transfer series of Co-Mabiq compounds with formal metal valencies of 0 → +2

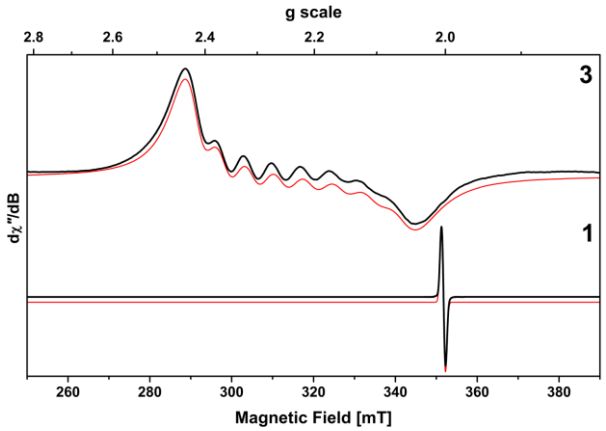

Fig. 1 X-band EPR spectra of **3** (CH_2Cl_2/toluene) and **1** (THF) Experimental data are represented by the black line and simulation by the red trace: **3**, g_{iso} = 2.224; A_{iso} = 74.2 × 10^{-4} cm^{-1}; **1**, g_{iso} = 2.0029; A_{iso} = 1.05 × 10^{-4} cm^{-1}.

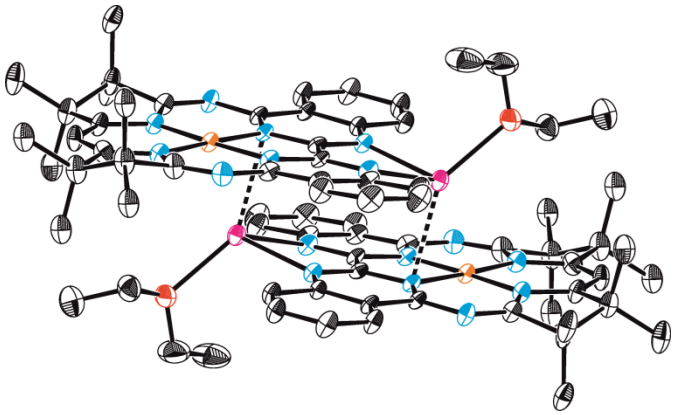

Fig. 2 Molecular structure of **1** (50% probability ellipsoids). Hydrogen atoms omitted for clarity.

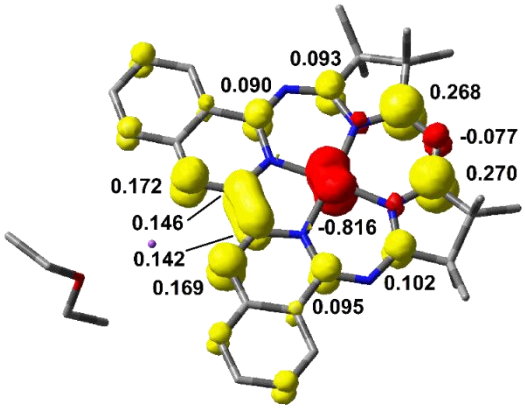

Fig. 3 DFT-derived (B3LYP) spin-density plot for the monomeric unit of **1** based on Löwdin population analysis.

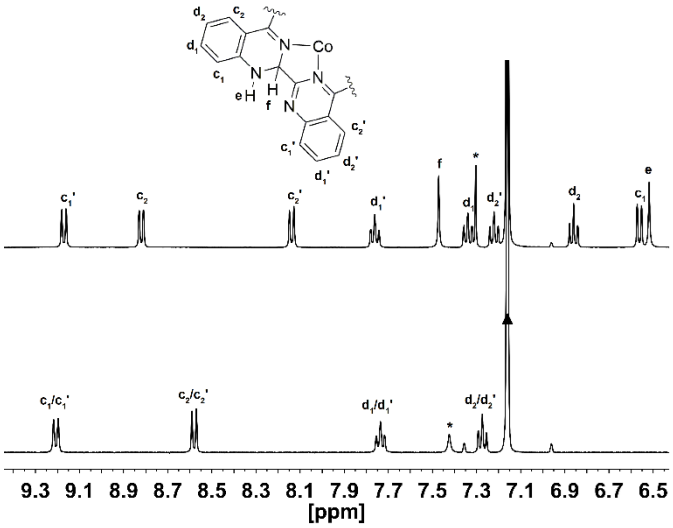

Fig. 4 ^{1}H NMR spectra (aromatic region; benzene-d_6 (▲)) of the two products of the **1**/benzoic reaction mixture: **2** (bottom) and (**[2-H₂]** (top). The diketiminate proton is denoted by the asterisk (*).

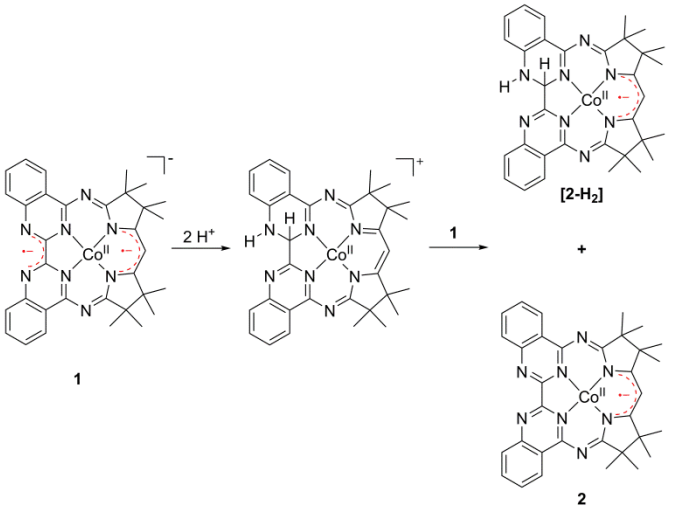

Scheme 2 Proposed reaction of **1** with acid to form **[2-H₂]**

Supplementary Information

A macrocyclic 'Co^{0}' complex: the relevance of ligand non-innocence to reactivity

Manuel Kaspar[†], Philipp J. Altmann[†], Alexander Pöthig[†], Stephen Sproules[§], Corinna R. Hess[†]*

[†]Department of Chemistry and Catalysis Research Center, Technische Universität München (TUM), Lichtenbergstrasse 4, D-85747 Garching, Germany

[§]WestCHEM, School of Chemistry, University of Glasgow, Glasgow, G12 8QQ, United Kingdom

Table of Contents

Experimental

Materials and methods

Chemicals were purchased from Sigma Aldrich and used as received unless otherwise noted. Metal compounds were synthesized in an inert atmosphere glove box (argon), using anhydrous solvents. The solvents were dried by passage over activated alumina columns from MBraun, deoxygenated by four freeze-pump-thaw cycles and stored over 3 Å (MeCN) or 4 Å activated molecular sieves. Triethylamine was degassed by sparging with argon and stored over 3 Å molecular sieves. $[Co(CH_3CN)_6](PF_6)_2$ was synthesized according to the literature procedure for the synthesis of $[Co(CH_3CN)_6](BF_4)_2$, using $NO(PF_6)$ instead of $NO(BF_4)$ as the oxidant.[1] *p*-Cyanoanilinium tetrafluoroborate (*p*CA) was prepared as described in the literature.[2] Tetrabutylammonium hexafluorophosphate was recrystallized in EtOH four times before use. Ferrocene was sublimed before use. H(Mabiq) and Co(Mabiq) were synthesized as previously described.[3-5]

Solution state NMR spectra were measured on a Bruker Avance Ultrashield (400 MHz ^1H) spectrometer. X-band EPR spectra were recorded on a Bruker ELEXSYS E500 spectrometer or on a JEOL JES-FA 200 spectrometer, and simulations performed with Bruker's Xsophe software package.[6] Electronic spectra were measured on a Shimadzu UV-3600 Plus UV-vis-NIR spectrophotometer or an Agilent Cary 60 UV-vis spectrophotometer. ESI mass spectra were measured on a Thermo Scientific™ UltiMate™ 3000 HPLC System using the loop mode. Microanalyses were carried out at the Technische Universität München. Electrochemical measurements were carried out with an EmStat^{3+} potentiostat using a three-electrode cell equipped with glassy carbon working electrode, a Pt wire counter electrode and a $Ag/AgNO_3$ reference electrode. Potentials are reported with reference to an internal standard of ferrocenium/ferrocene ($Fc^{+/0}$).

Single crystal X-ray diffraction

General: For crystallization, pentane was allowed to diffuse slowly into a THF solution of compound **1**. Compound **2** was crystallized by slow evaporation of a concentrated Et_2O solution. Data were collected on an X-ray single crystal diffractometer equipped with a CMOS detector (Bruker Photon-100), a rotating anode (Bruker TXS) with MoK_α radiation ($\lambda = 0.71073$ Å) and a Helios mirror optic by using the APEX III software package.[7] The measurements were performed on a single crystal coated with perfluorinated ether. The crystal was fixed on top of a microsampler and transferred to the diffractometer. The crystal was frozen under a stream of cold nitrogen. A matrix scan was used to determine the initial lattice parameters. Reflections were merged and corrected for Lorentz and polarization effects, scan speed, and background using SAINT.[8] Absorption corrections, including odd and even ordered spherical harmonics, were performed using SADABS.[8] Space group assignments were based upon systematic absences, E statistics, and successful refinement of the structures. Structures were solved by direct methods with the aid of successive difference Fourier maps, and were refined against all data using SHELXLE[9] in conjunction with SHELXL-2014[10]. Hydrogen atoms were assigned to ideal positions and refined using a riding model with an isotropic thermal parameter 1.2 times that of the attached carbon atom (1.5 times for methyl hydrogen atoms). If not mentioned otherwise, non-hydrogen atoms were refined with anisotropic displacement parameters. Full-matrix least-squares refinements were carried out by minimizing $\Sigma w(Fo^2-Fc^2)^2$ with SHELXL-97[11] weighting scheme. Neutral atom scattering factors for all atoms and anomalous dispersion corrections for the non-hydrogen atoms were taken from International Tables for Crystallography.[12] Images of the crystal structures were generated by PLATON.[13-14]

Special:

[Co(Mabiq)(THF)](PF$_6$) (3): Geometrical restraints have been applied for disordered PF_6^- anions (see CIF).

[Co(Mabiq)Na(OEt)]$_2$ (1): Geometrical restraints have been applied for disordered parts of the ligand (see CIF). The unit cell contains four diethyl ether molecules close to a special position, which have been treated as a diffuse contribution to the overall scattering without specific atom positions by PLATON/SQUEEZE.[15]

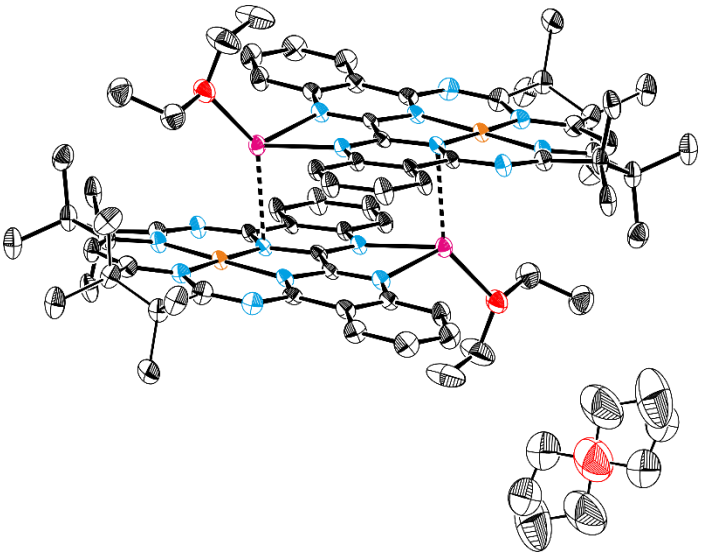

The above figure shows the ORTEP style representation of **1** with one equivalent of diethyl ether co-crystallized close to a special position, which has been treated as a diffuse contribution to the overall scattering without specific atom positions by PLATON/SQUEEZE[15] in the subsequent refinement process. Ellipsoids are shown at the 50% probability level. Hydrogen atoms are omitted for clarity.

Density Functional Theory calculations

Density Functional Theory (DFT) calculations were performed with the ORCA program package.[16] Geometry optimizations of the complexes were performed at the B3LYP[17-19] level of DFT. The all-electron Gaussian basis sets were those developed by the Ahlrich's group.[20-21] Triple-ζ quality basis sets (TZV(P)) with one set of polarization functions on the metals and on the atoms directly coordinated to the metal center were used.[21] For the carbon and hydrogen atoms, slightly smaller polarized split-valence SV(P) basis sets were used that were of double-ζ quality in the valence region and contained a polarizing set of d functions on the non-hydrogen atoms. Auxiliary basis sets used to expand the electron density in the resolution-of-the-identity (RI) approach were chosen,[22-23] where applicable, to match the orbital basis. SCF calculations were tightly converged (1×10^{-8} E_h in energy, 1×10^{-7} E_h in the density change, and 1×10^{-7} E_h in maximum element of the DIIS error vector). Geometry optimizations were carried out in redundant internal coordinates without imposing symmetry constraints. In all cases the geometries were considered converged after the energy change was less than 5×10^{-6} E_h, the gradient norm and maximum gradient element were smaller than 1×10^{-4} and 3×10^{-4} E_h $Bohr^{-1}$, respectively, and the root-mean square and maximum displacements of all atoms were smaller than 2×10^{-3} and 4×10^{-3} Bohr, respectively. Orbital/spin density plots were created using GaussView.[24]

Syntheses

[Co(Mabiq)Na(OEt$_2$)]$_2$ (1). Sodium (3.3 mg, 0.14 mmol) was added to a solution of Co(Mabiq) (86.2 mg, 0.14 mmol) in THF (10 mL) and the mixture was stirred for 48 h. The resultant dark red solution was filtered through celite and the solvent evaporated. The crude product was dissolved in ether and precipitated with hexane to give a dark red solid (80 mg, 80% yield). Single crystals were grown by slow evaporation of a concentrated solution of **1** in Et_2O.

Anal. Calcd. for Co(Mabiq)Na(OEt$_2$), $C_{37}H_{43}Co\ N_8NaO$: C, 63.69; H, 6.21; N, 16.06. Found: C, 63.51; H, 6.19; N, 15.95.

UV-Vis λ_{max} (nm (ε, $M^{-1}\ cm^{-1}$)) in THF: 340 (3.6×10^4), 401 (2.6×10^4), 442 (1.6×10^4), 534 (1.5×10^4), 870 (3.4×10^3), 1038 (2.1×10^3), 1206 (1.9×10^3).

[Co(Mabiq)(THF)](PF$_6$) (3). [Co(CH$_3$CN)$_6$](PF$_6$)$_2$ (105 mg, 0.18 mmol) was added to a suspension of HMabiq (96 mg, 0.18 mmol) and triethylamine (26 µL, 0.19 mmol) in MeCN (5 mL). The suspension was stirred overnight and the resultant brown mixture was filtered through celite. After evaporation of the solvent, the crude product was dissolved in DCM and precipitated with hexane to give a red solid (120 mg, 82% yield). Single crystals were obtained by slow diffusion of pentane into a concentrated solution of **3** in THF.

Anal. Calcd. for $C_{37}H_{41}CoF_6N_8OP$: C, 54.35; H, 5.05; N, 13.70. Found: C, 54.24; H, 5.08; N, 13.46.

ESI-MS(+) (*m/z*): 600.65 $[M-(THF + PF_6)]^+$.

UV-Vis λ_{max} (nm (ε, $M^{-1}\ cm^{-1}$)) in THF: 316 (3.1×10^4), 429 (9.5×10^3), 570 (3.5×10^3), 607 (2.7×10^3), 658 (1.3×10^3).

General procedure for reactions of 1 and 2 with acid (*p*CA, benzoic acid)

All reactions were carried out in an inert atmosphere (argon) glovebox. 0.5 mL of **1** or **2** (0.015 M solution in THF-d_8) were placed in a J-Young NMR tube and frozen. Subsequently, 20 or 100 µL (1 or 5 equiv.) of a 0.36 M solution of acid in THF-d_8 were added to the frozen sample. The NMR tube was sealed and kept frozen until the measurement of the NMR spectrum. Aliquots of each reaction mixture were analyzed by absorption spectroscopy and ESI mass spectrometry.

Alternatively, 0.5 mL of **1** or **2** (0.015 M solution in THF) were placed in a vial and 20 or 100 µL (1 or 5 equiv.) of a 0.36 M solution of acid in THF were added. The mixtures were stirred for 30 min and analyzed by absorption spectroscopy and ESI mass spectrometry.

Isolation of [2-H_2] from the 1/benzoic acid reaction

Compound **1** (70 mg, 0.1 mmol) was dissolved in THF (5 mL) and a solution of benzoic acid (61 mg, 0.5 mmol) in THF (1 mL) was added. The reaction mixture was stirred for 30 min, filtered and the solvent removed in vacuo. The solid was subsequently washed with MeCN to remove excess benzoic acid. The remaining purple solid was a mixture of **2** and **[2-H_2]**, from which **[2-H_2]** was separated by column chromatography (THF:hexane = 1:6, R_f = 0.43, silica gel , pore size 60 Å, 230-400 mesh particle size, 40-63 µm) as a purple solid (21 mg, 35% yield). Single crystals of **[2-H_2]** were obtained by slow diffusion of pentane into a concentrated solution of **[2-H_2]** in THF.

^{1}H NMR (400 MHz, benzene-d_6, 25 °C, TMS): δ= 1.16 (s, 3H, CH_3, H_a), 1.26 (s, 3H, CH_3, H_a), 1.27 (s, 3H, CH_3, H_a), 1.28 (s, 3H, CH_3, H_a), 1.33 (s, 3H, CH_3, H_a), 1.34 (s, 3H, CH_3, H_a), 1.38 (s, 3H, CH_3, H_a), 1.39 (s, 3H, CH_3, H_a), 6.52 (s, 1H, NH, H_e), 6.56 (dd, J = 8.0, 1.1 Hz, 1H, CH, H_c), 6.89 - 6.82 (m, 1H, CH, H_d), 7.22 (ddd, J = 8.1, 6.9, 1.1 Hz, 1H, CH, $H_{d'}$), 7.30 (s, 1H, CH, H_b), 7.34 (m, 1H, CH, H_d),

7.47 (s, 1H, CH, H_f), 7.76 (ddd, *J* = 8.2, 6.9, 1.4 Hz, 1H, CH, $H_{d'}$), 8.14 (d, *J* = 8.1 Hz, 1H, CH, $H_{c'}$), 8.82 (dd, *J* = 7.8, 1.4 Hz, 1H, CH, H_c), 9.17 (dd, *J* = 8.2, 1.3 Hz, 1H, CH, $H_{c'}$).

Table S1. Crystallographic data for **3** and **1** at 100K.

	3	**1**
Empirical formula	$4(C_{37}H_{41}CoN_8O)$, $4(F_6P)$, C_4H_8O	$C_{74}H_{86}Co_2N_{16}Na_2O_2$
Formula weight	3342.82	1395.43
Crystal system	monoclinic	monoclinic
Space group	*C* 2/*c*	*P* 2_1/*c*
a (Å)	71.25(3)	12.6857(8)
b (Å)	10.283(4)	14.0773(10)
c (Å)	20.132(8)	21.3596(13)
α (°)	90	90
β (°)	91.821(3)	99.336(2)
γ (°)	90	90
Volume ($Å^3$)	14743(10)	3763.9(4)
Z	4	2
ρ_{calc} (mg/mm^3)	1.506	1.231
μ (mm^{-1})	0.585	0.507
F(000)	6928	1468
Reflections collected	57304	116385
Independent refl., R_{int}	12999, 0.0955	6647, 0.0796
Data/restraints/parameters	12999/262/1141	6647/137/502
Goodness-of-fit on F^2	1.057	1.137
Final R_1 indexes [$I \geq 2\sigma(I)$]	0.0594	0.0643
Final wR_2 indexes [all data]	0.1425	0.1698
$\Delta\rho_{min,max}$ (e $Å^{-3}$)	0.741/-0.651	0.906/-0.538

Table S2. Select bond distances for **3** and **1**.

	3[a]	**1**
Co1–N1	1.915(3) (Co2–N10 1.920(3))	1.890(3)
Co1–N2	1.918(3) (Co2–N9 1.913(3))	1.890(3)
Co1–N3	1.899(3) (Co2–N12 1.898(3))	1.868(3)
Co1–N4	1.896(3) (Co2–N11 1.887(4))	1.878(3)
N3–C13	1.347(5) (N12–C52 1.350(5))	1.361(5)
C13–C14	1.388(6) (C52–C51 1.391(6))	1.392(6)
C14–C15	1.387(6) (C51–C50 1.379(6))	1.374(6)
N4–C15	1.354(5) (N11–C50 1.350(5))	1.367(5)
C9–N2	1.341(5) (N9–C56 1.346(5))	1.355(5)
N2–C2	1.394(5) (N9–C38 1.380(5))	1.400(5)
C2–N6	1.299(5) (C38–N13 1.300(5))	1.347(5)
N6–C3	1.370(5) (N13–C62 1.380(5))	1.365(5)
C2–C1	1.476(5) (C38–C39 1.491(6))	1.422(5)
C19–N1	1.345(5) (C46–N10 1.348(5))	1.350(5)
N1–C1	1.377(5) (N10–C39 1.376(5))	1.396(5)
C1–N5	1.303(5) (C39–N14 1.300(5))	1.328(5)
N5–C25	1.378(5) (N14–C40 1.374(5))	1.373(5)
Na1–N5		2.335(5)
Na1–N6		2.381(5)
Na1–N1a		2.676(4)

[a] the asymmetric unit of **3** contains two independent molecules. The corresponding values for the second molecule are therefore are also given, in parentheses.

Table S3. DFT-derived (B3LYP, UKS) Löwdin atomic charges and spin populations for the monomeric unit of **1**.

LOEWDIN ATOMIC CHARGES AND SPIN POPULATIONS

---

0 Co:	0.203739	-0.816272
1 Na:	0.561383	0.002865
2 O :	-0.510054	-0.000041
3 N :	-0.524272	0.171834
4 N :	-0.334200	0.015500
5 N :	-0.463625	-0.013663
6 N :	-0.357907	-0.014087
7 N :	-0.355380	-0.017871
8 N :	-0.463054	-0.015552
9 N :	-0.337051	0.019538
10 N :	-0.524120	0.169344
11 C :	0.266964	0.145579
12 C :	0.144285	-0.013562
13 C :	-0.135262	0.067259
14 C :	-0.108143	-0.007405
15 C :	-0.147193	0.071894
16 C :	-0.088307	-0.000909
17 C :	-0.021925	0.042405
18 C :	0.295532	0.090286
19 C :	0.309011	0.092826
20 C :	-0.041985	0.001927
21 C :	-0.289496	0.000492
22 C :	-0.288040	0.005560
23 C :	-0.050619	-0.002990
24 C :	-0.289918	0.014472
25 C :	-0.296877	0.003772
26 C :	0.136131	0.268386
27 C :	-0.168528	-0.077270
28 C :	0.136224	0.269745
29 C :	-0.050629	-0.002919
30 C :	-0.290046	0.014553
31 C :	-0.296607	0.003799
32 C :	-0.041944	0.001623
33 C :	-0.289465	0.000704
34 C :	-0.288124	0.006040
35 C :	0.306546	0.102113
36 C :	0.294418	0.095657
37 C :	-0.021523	0.040438
38 C :	-0.088203	0.001405

39	C :	-0.147120	0.069999
40	C :	-0.108716	-0.004848
41	C :	-0.137463	0.065752
42	C :	0.143635	-0.011571
43	C :	0.268444	0.142056
44	C :	-0.313234	0.000085
45	C :	0.013416	0.000023
46	C :	0.014440	0.000014
47	C :	-0.323159	-0.000006
48	H :	0.120654	-0.002136
49	H :	0.114837	0.000230
50	H :	0.116021	-0.002360
51	H :	0.136615	0.000076
52	H :	0.115021	0.000047
53	H :	0.122067	0.000094
54	H :	0.107191	0.000208
55	H :	0.120781	-0.000118
56	H :	0.115629	-0.000112
57	H :	0.109934	0.000536
58	H :	0.117140	-0.000380
59	H :	0.110118	0.002634
60	H :	0.111585	-0.000057
61	H :	0.114308	0.000239
62	H :	0.111160	-0.000079
63	H :	0.112454	0.000519
64	H :	0.122693	0.002391
65	H :	0.117146	-0.000371
66	H :	0.111543	-0.000093
67	H :	0.110162	0.002592
68	H :	0.112290	0.000542
69	H :	0.110987	-0.000074
70	H :	0.114207	0.000244
71	H :	0.122096	0.000084
72	H :	0.114910	0.000038
73	H :	0.106900	0.000229
74	H :	0.120632	-0.000139
75	H :	0.109887	0.000551
76	H :	0.115485	-0.000104
77	H :	0.136548	0.000004
78	H :	0.116028	-0.002297
79	H :	0.114988	0.000146
80	H :	0.121690	-0.002084
81	H :	0.142112	-0.000010
82	H :	0.139441	0.000013
83	H :	0.134789	0.000010
84	H :	0.113135	0.000000

85	H :	0.114371	0.000009
86	H :	0.129079	-0.000004
87	H :	0.115068	0.000001
88	H :	0.127504	0.000001
89	H :	0.129184	-0.000000
90	H :	0.119633	0.000001

Table S4. DFT-optimized (B3LYP, UKS) geometry (.XYZ format) for the monomeric unit of **1**.

CARTESIAN COORDINATES (ANGSTROEM)

Co	0.097797	0.117993	-0.168999
Na	0.374752	-5.527592	-0.230111
O	0.626188	-7.791673	-0.561952
N	-1.122565	-3.790384	-0.248507
N	-1.121508	-1.363234	-0.259888
N	-3.176049	-0.180010	-0.406245
N	-1.350033	1.361575	-0.124509
N	1.415329	1.497530	-0.069812
N	3.391791	0.138629	-0.264154
N	1.455849	-1.236551	-0.198962
N	1.690660	-3.651472	-0.164765
C	-0.485507	-2.601909	-0.231377
C	-2.486877	-3.787959	-0.301818
C	-3.204564	-5.012849	-0.315473
C	-4.591788	-5.024234	-0.375702
C	-5.314580	-3.816876	-0.424975
C	-4.629296	-2.603736	-0.412952
C	-3.224493	-2.571478	-0.351031
C	-2.463802	-1.322865	-0.332869
C	-2.654241	1.012868	-0.325424
C	-3.528487	2.253022	-0.523069
C	-4.955999	2.081261	0.010367
C	-3.598854	2.501364	-2.051475
C	-2.657706	3.338275	0.210293
C	-2.976879	3.393210	1.726966
C	-2.787972	4.758023	-0.362450
C	-1.268802	2.722410	0.053531
C	-0.070376	3.414864	0.162547
C	1.194207	2.843017	0.098311
C	2.508160	3.592551	0.311279
C	2.750603	3.683935	1.840413
C	2.521021	5.016175	-0.266592
C	3.513043	2.595690	-0.374750
C	4.923988	2.562422	0.224691
C	3.629471	2.846836	-1.899486
C	2.754639	1.276617	-0.210239
C	2.791425	-1.066556	-0.214680
C	3.668286	-2.236327	-0.186772
C	5.071200	-2.135086	-0.187725
C	5.868858	-3.277195	-0.151367
C	5.263702	-4.547608	-0.111248

C	3.880004	-4.668534	-0.111321
C	3.049512	-3.517708	-0.152388
C	0.942159	-2.531519	-0.192741
C	1.300112	-7.160928	-2.791343
C	1.084221	-8.310705	-1.822687
C	0.397005	-8.785925	0.452822
C	-0.920650	-9.535136	0.289249
H	-2.640887	-5.952434	-0.278379
H	-5.126493	-5.980131	-0.385331
H	-6.407479	-3.831734	-0.472885
H	-5.165342	-1.654015	-0.451355
H	-4.977018	1.735797	1.055767
H	-5.494799	1.331109	-0.591283
H	-5.510644	3.035972	-0.054732
H	-4.043801	1.620793	-2.545848
H	-2.599139	2.668641	-2.488634
H	-4.228997	3.378061	-2.283511
H	-2.929628	2.393210	2.191837
H	-3.982131	3.812577	1.910888
H	-2.240744	4.035834	2.240851
H	-2.414309	4.835156	-1.396226
H	-2.223550	5.482281	0.251549
H	-3.844517	5.083381	-0.351804
H	-0.127397	4.493593	0.319536
H	2.779281	2.685625	2.310400
H	1.932138	4.252783	2.315067
H	3.700414	4.200201	2.067166
H	3.536738	5.449228	-0.210488
H	1.856872	5.680790	0.314311
H	2.189642	5.050243	-1.316880
H	5.555379	1.857267	-0.340365
H	4.927975	2.231162	1.274823
H	5.393687	3.562409	0.170355
H	4.184748	2.015537	-2.366522
H	4.175868	3.783647	-2.107939
H	2.639161	2.908121	-2.383508
H	5.516248	-1.139094	-0.216454
H	6.959242	-3.187173	-0.151615
H	5.887035	-5.447721	-0.078336
H	3.406268	-5.656098	-0.074751
H	2.056483	-6.448304	-2.414576
H	0.357823	-6.616789	-2.986972
H	1.663758	-7.550650	-3.758176
H	0.338798	-9.021431	-2.227031
H	2.027962	-8.867273	-1.654761
H	0.405630	-8.234462	1.409005

H	1.254648	-9.486405	0.467310
H	-1.773639	-8.833663	0.277301
H	-1.058625	-10.228022	1.138876
H	-0.949133	-10.134955	-0.637051

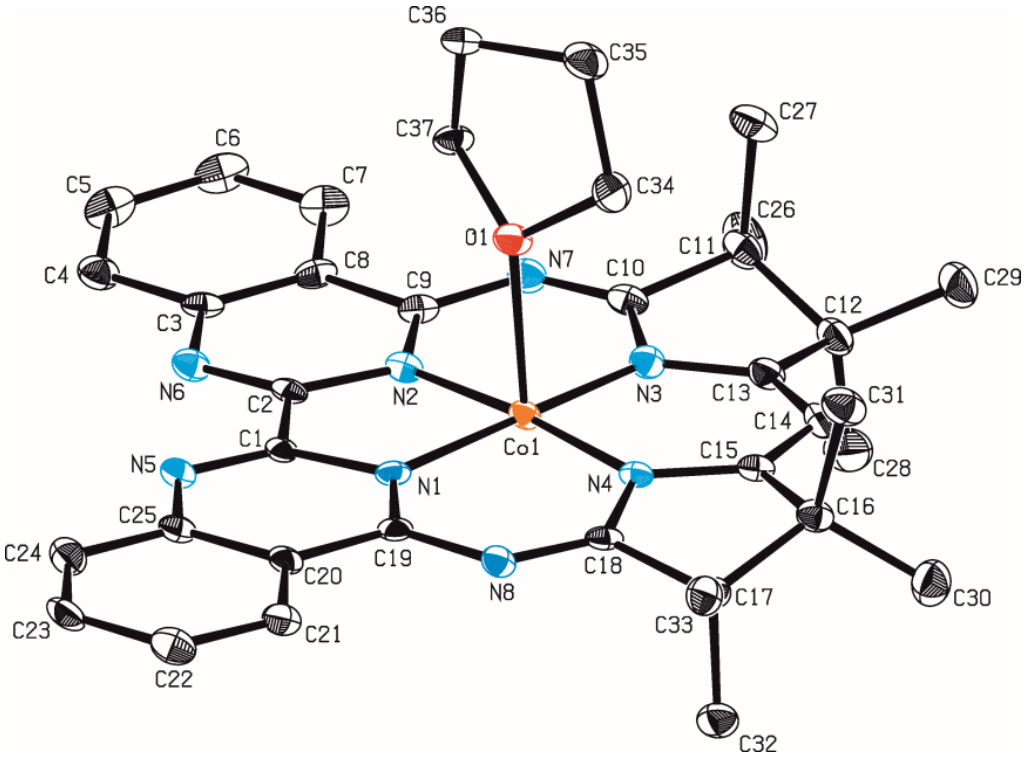

Figure S1. ORTEP style representation of **3** (one of two molecules in the asymmetric unit). Ellipsoids are shown at the 50% probability level. Hydrogen atoms are omitted for clarity.

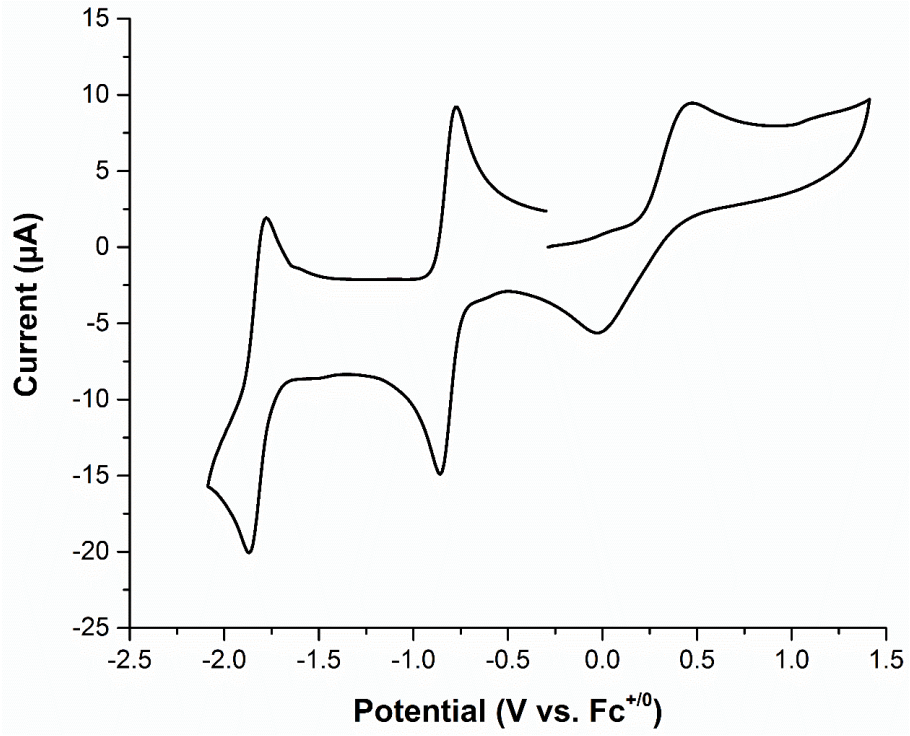

Fig. S2. Cyclic voltammogram of **3** (0.84 mM) in MeCN; 0.1 M $[N(n\text{-}Bu)_4]PF_6$; scan rate: 0.1 V/s.

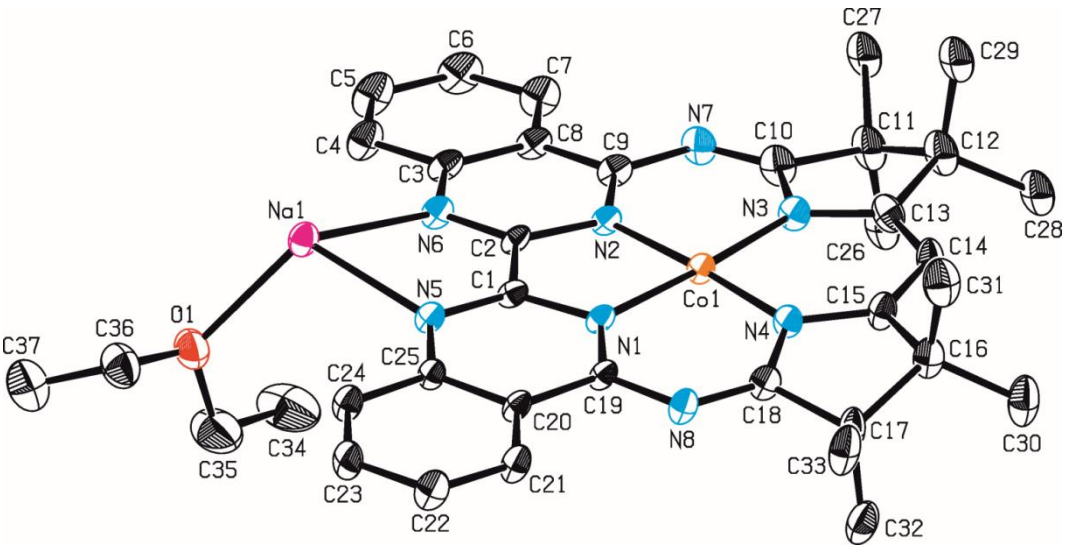

Figure S3. ORTEP style representation of the monomeric unit of **1**. Ellipsoids are shown at the 50% probability level. Hydrogen atoms omitted for clarity.

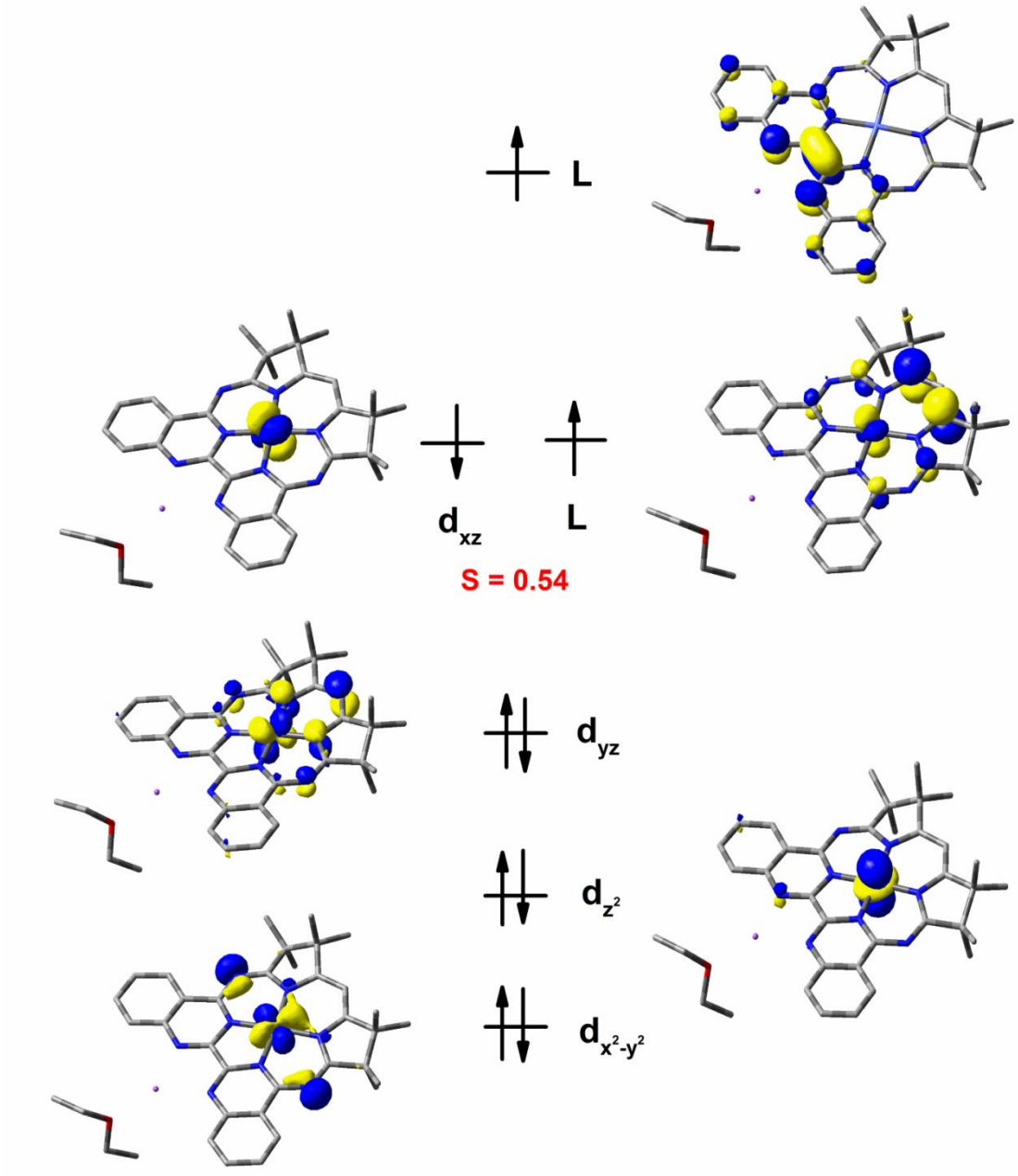

Figure S4. DFT-derived (B3LYP) qualitative molecular orbital diagram of the monomeric unit ([Co(Mabiq)Na(OEt_2)]) of **1**.

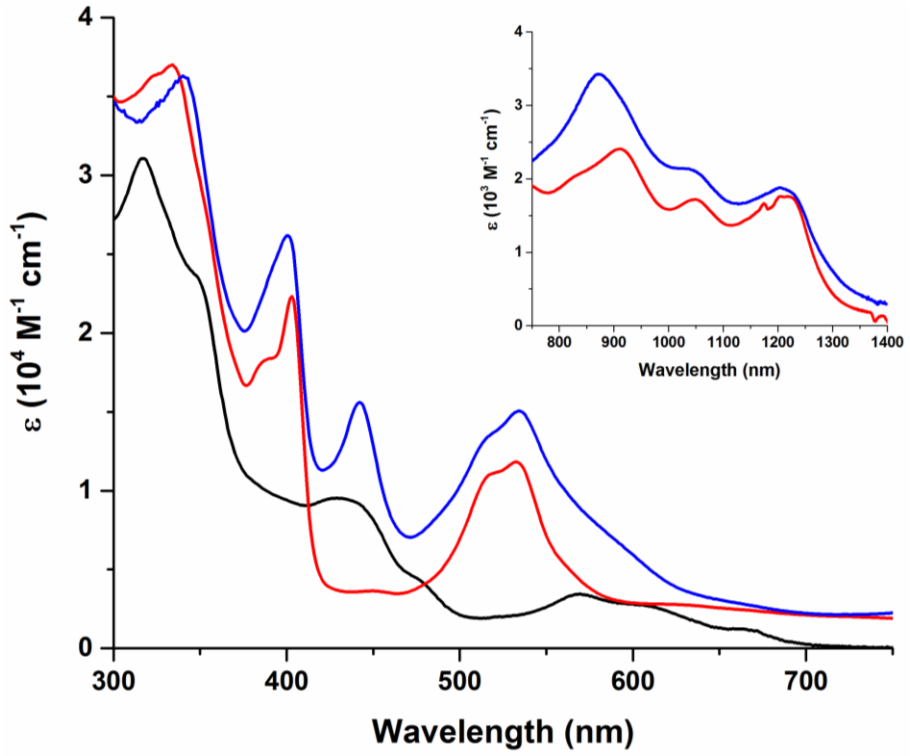

Fig. S5. Electronic spectra of **1** (blue), **2** (red) and **3** (black) in THF. Inset NIR region of the spectra of **1** and **2**.

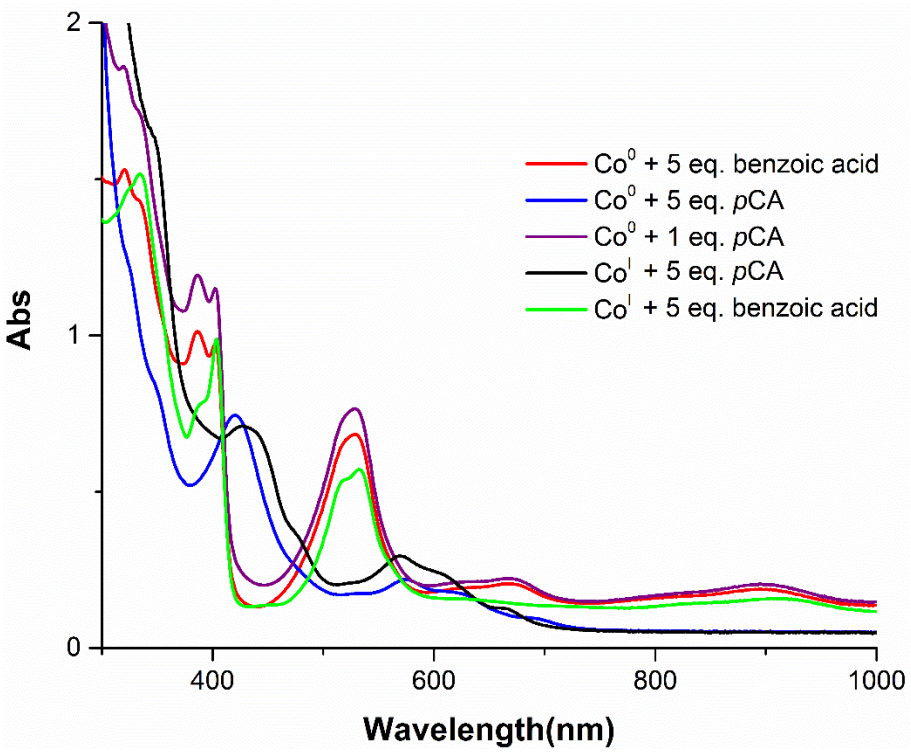

Figure S6. UV-vis spectra of the reaction products of **1** and **2** with *p*CA and benzoic acid.

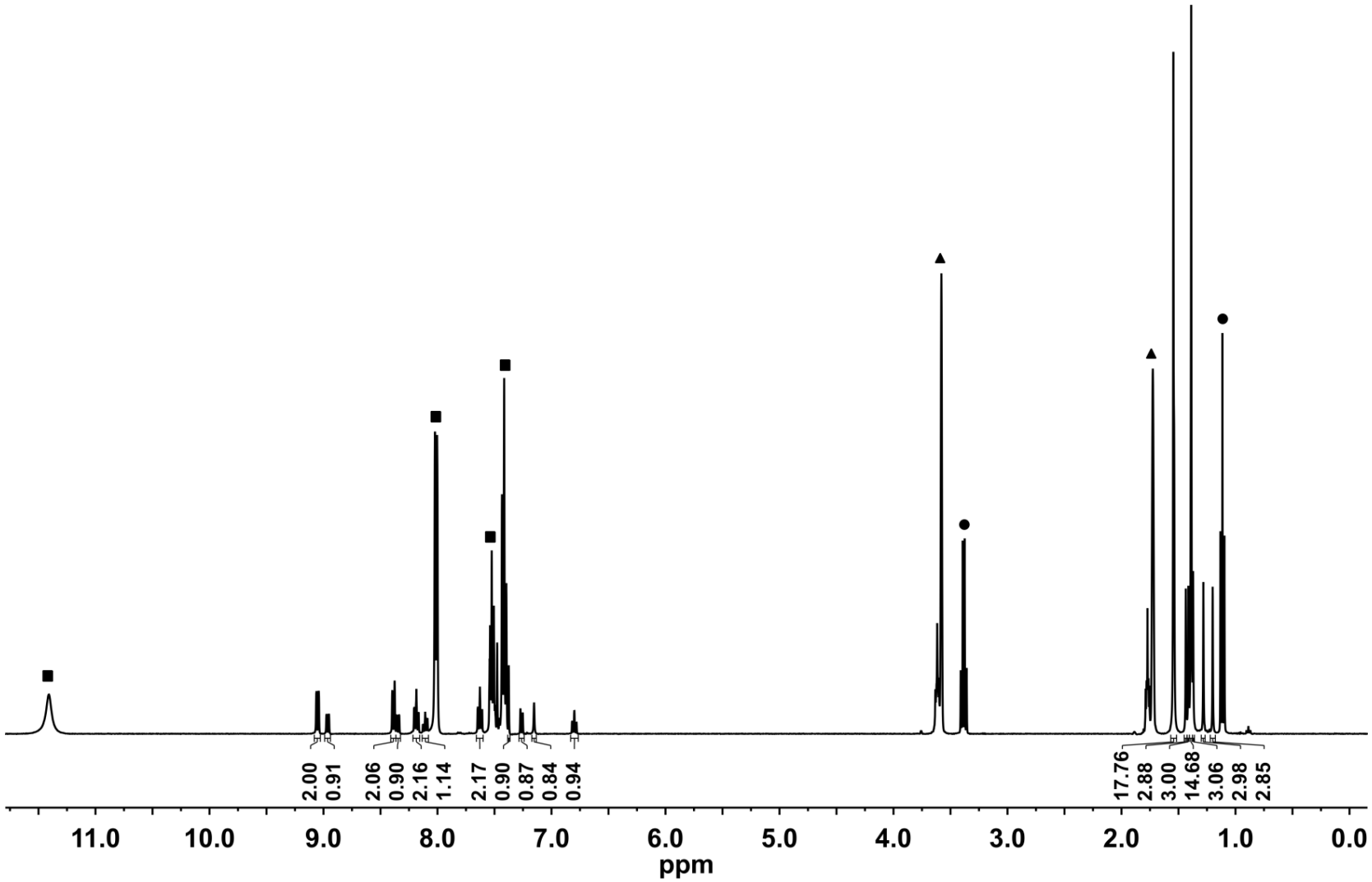

Figure S7. Full ^{1}H NMR spectrum for the product of **1** ([Co] = 0.015 mM) plus 5 equiv. benzoic acid in THF-d_8; ■ benzoic acid, ● Et_2O, ▲ THF-d_8.

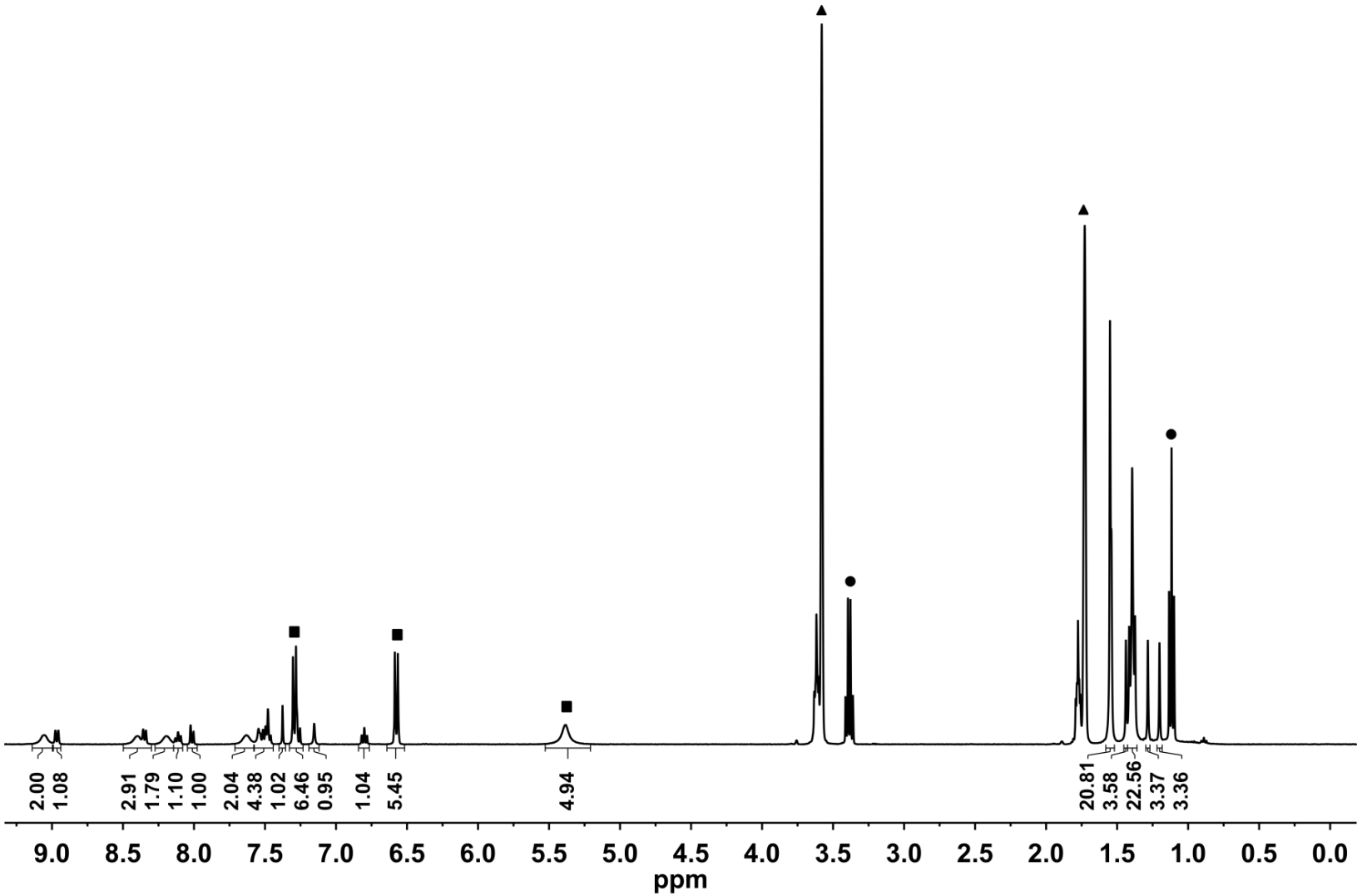

Figure S8. Full ^{1}H NMR spectrum for the product of **1** ([Co] = 0.015 mM) plus 1 equiv. *p*-cyanoaniline in THF-d_8; ■ *p*CA, ● Et_2O, ▲ THF-d_8.

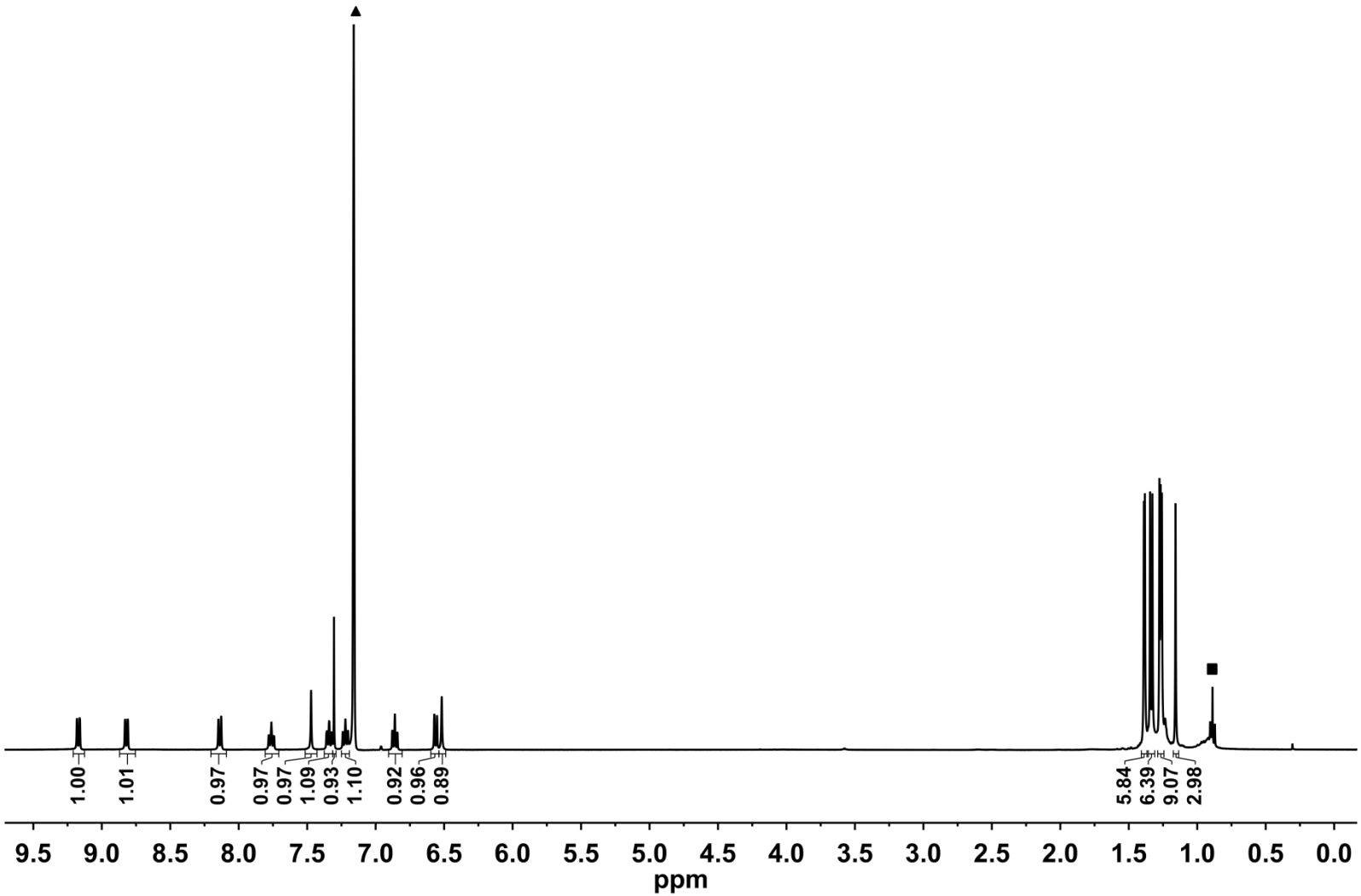

Figure S9. Full ^{1}H NMR spectrum of. [**2-H$_2$**] in benzene-d$_6$; ▲ benzene-d$_6$, ■ hexane.

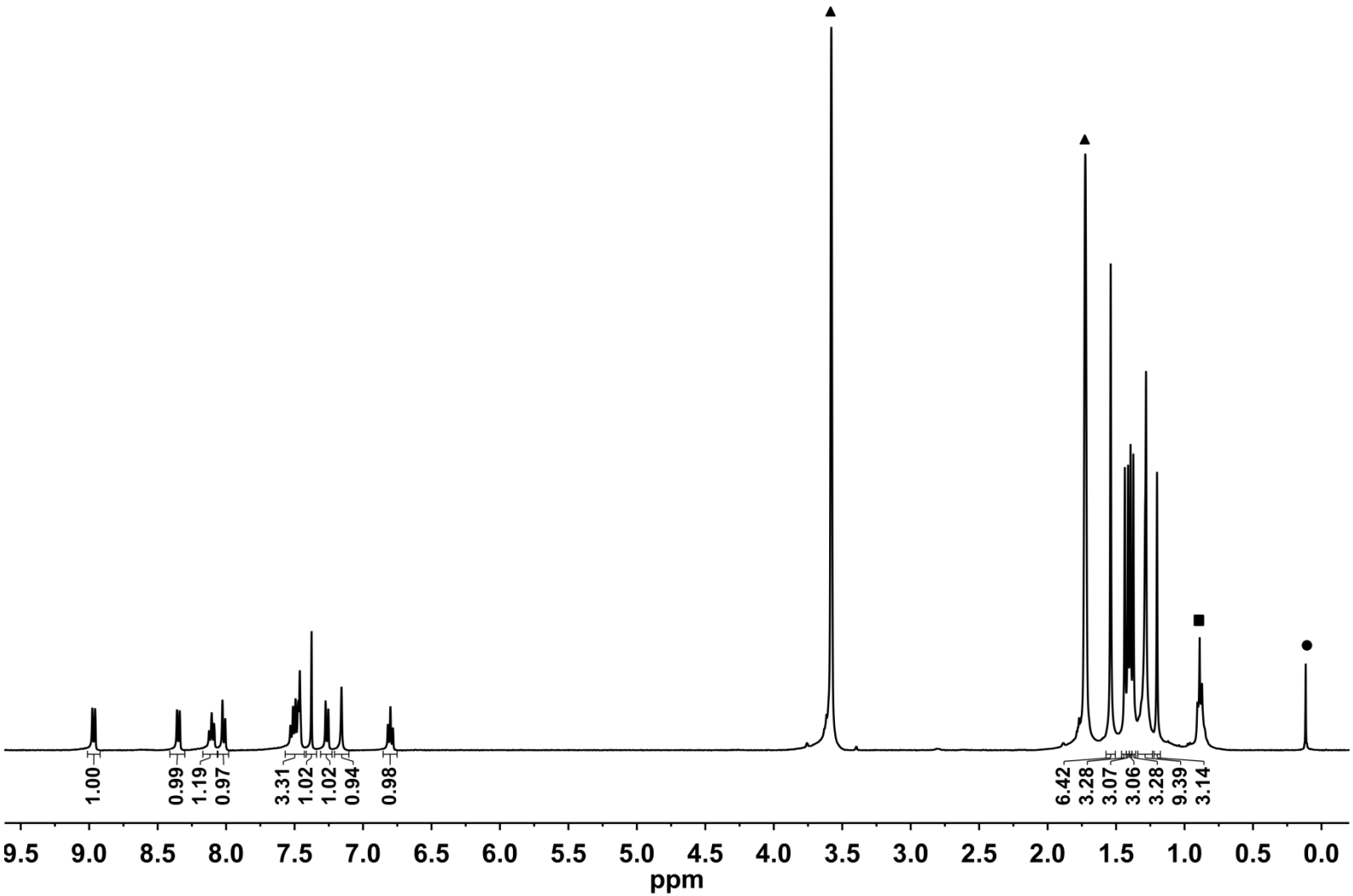

Figure S10. Full ^{1}H NMR spectrum of. [**2-H$_2$**] in THF-d$_8$; ▲ THF-d$_8$, ■ hexane, ▲silicon grease.

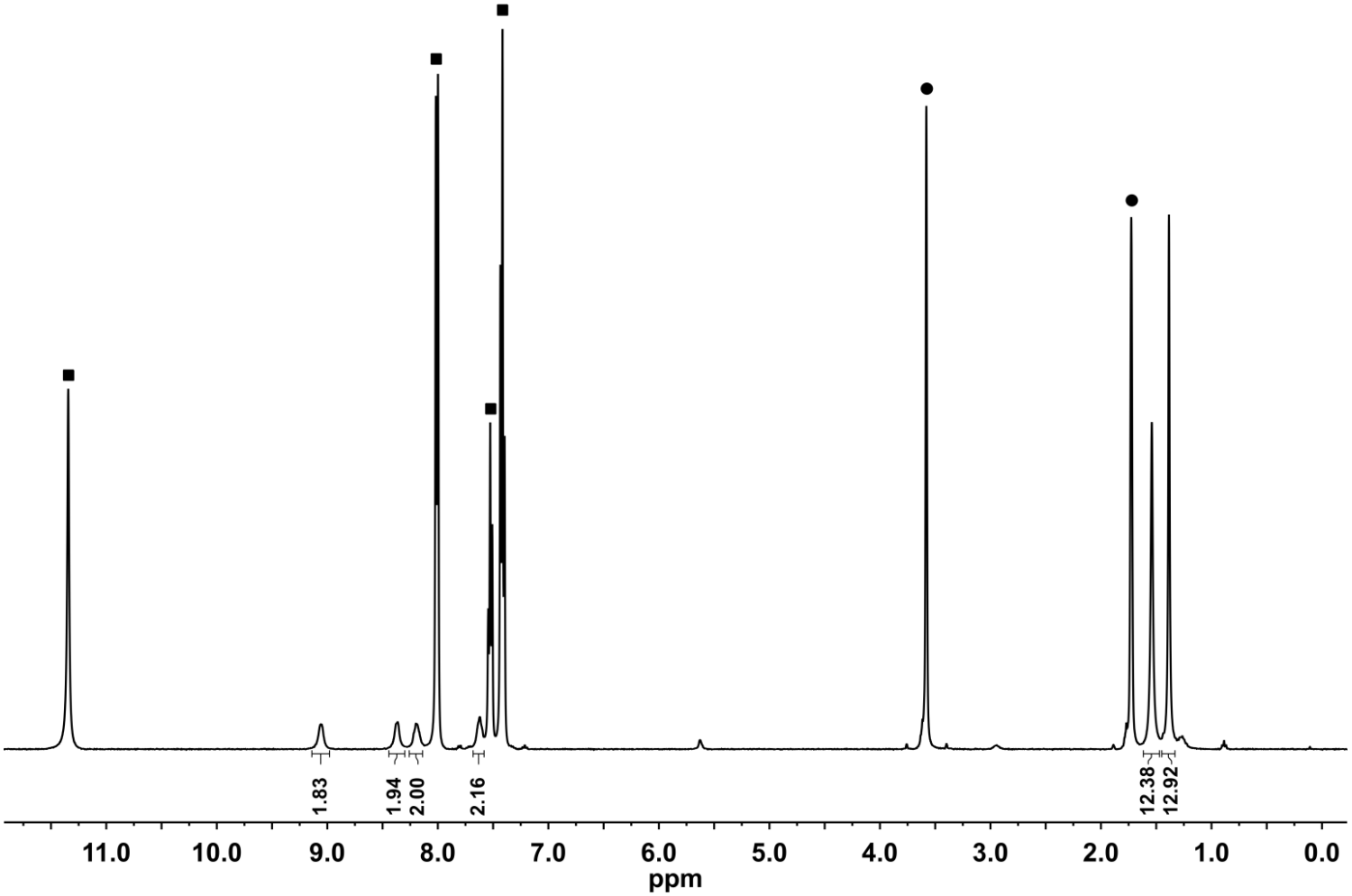

Figure S11. ^{1}H NMR spectrum of a mixture of **2** and 5 equiv. benzoic acid in THF-d_8; ■ benzoic acid, ● THF-d_8.

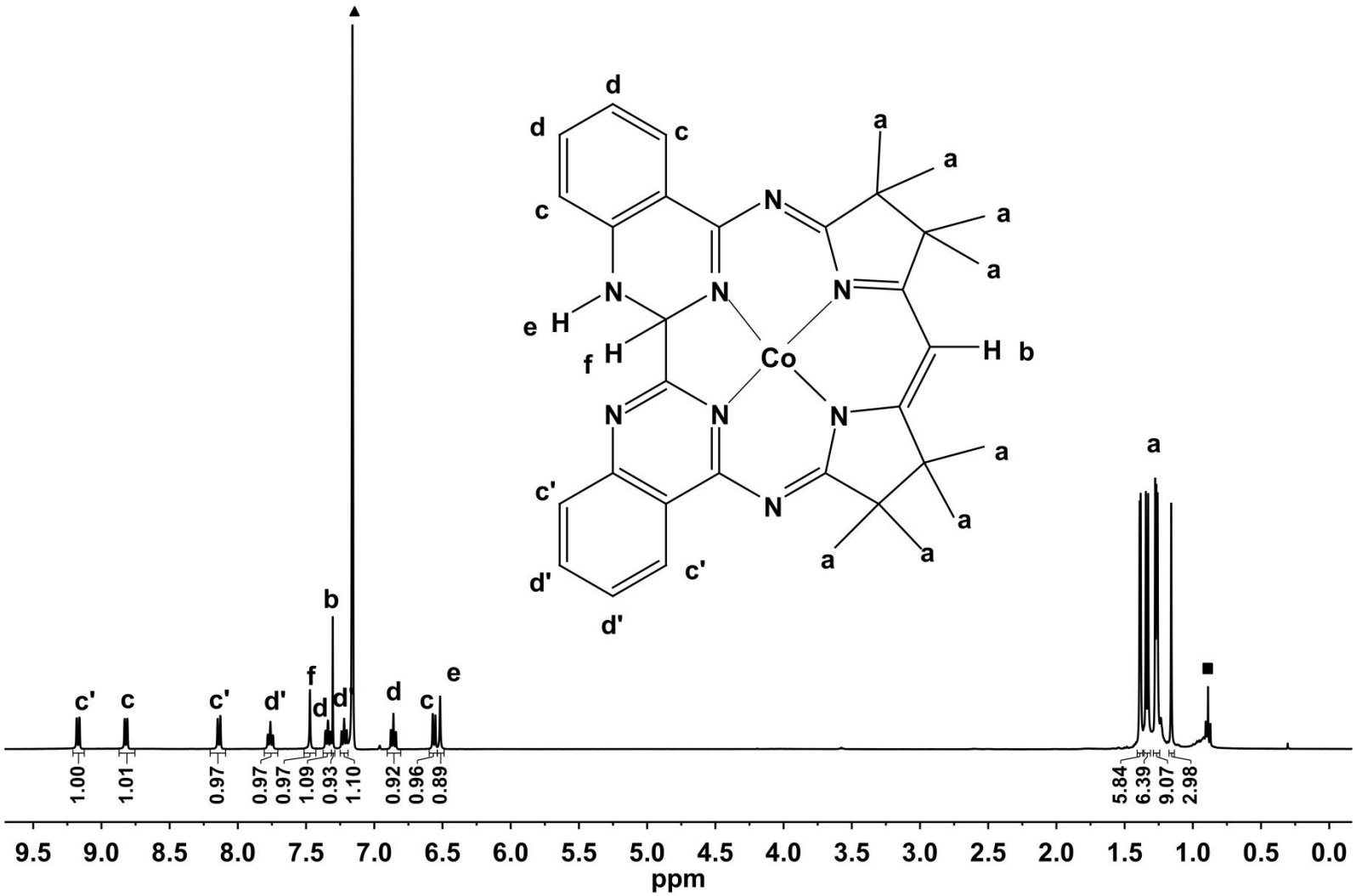

Figure S12. ^{1}H NMR spectrum of. [**2-H$_2$]** including proton assignments; ▲ benzene-d$_6$, ■ hexane.

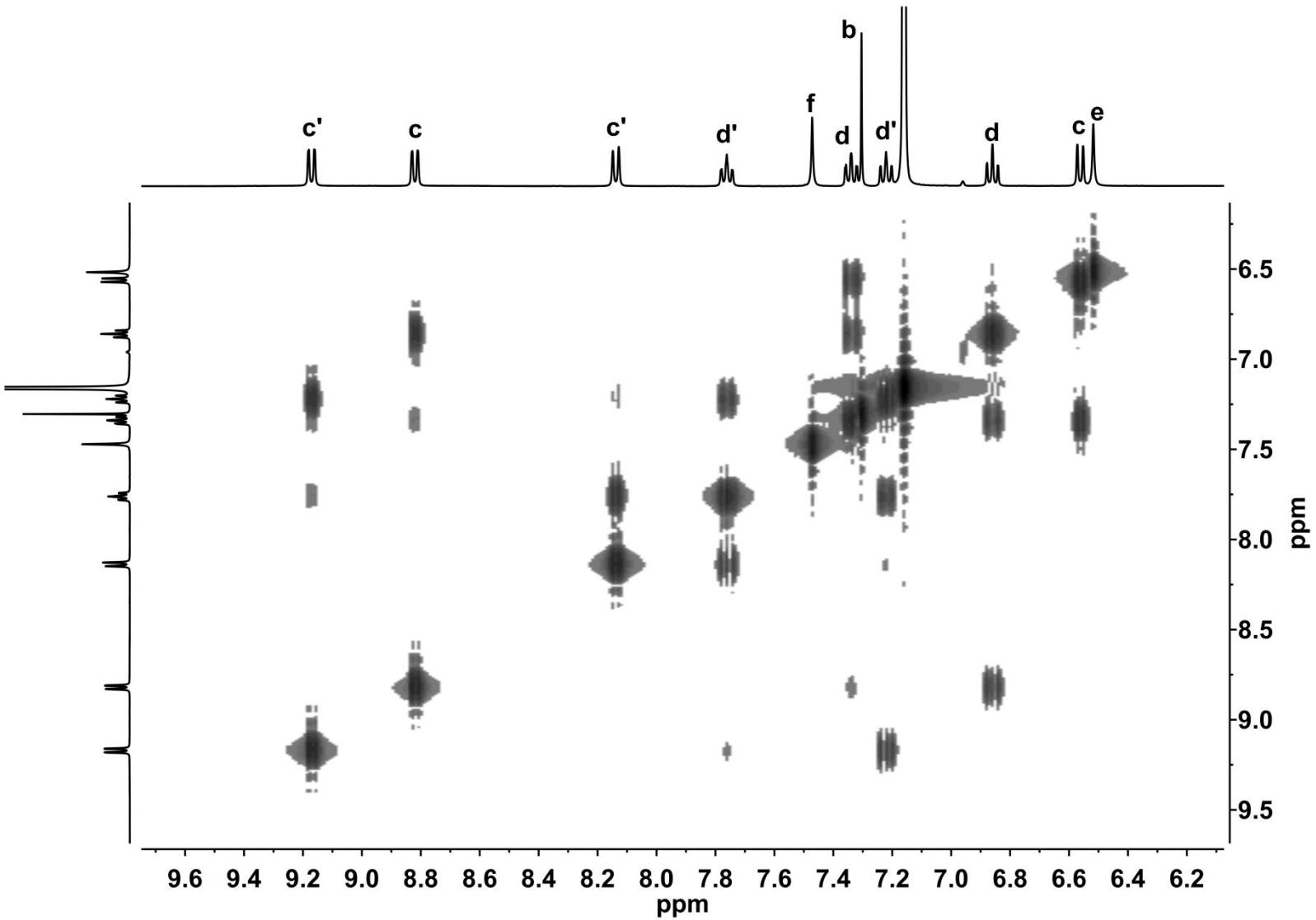

Figure S13. COSY NMR spectrum of. [**2-H$_2$**] in benzene-d$_6$.

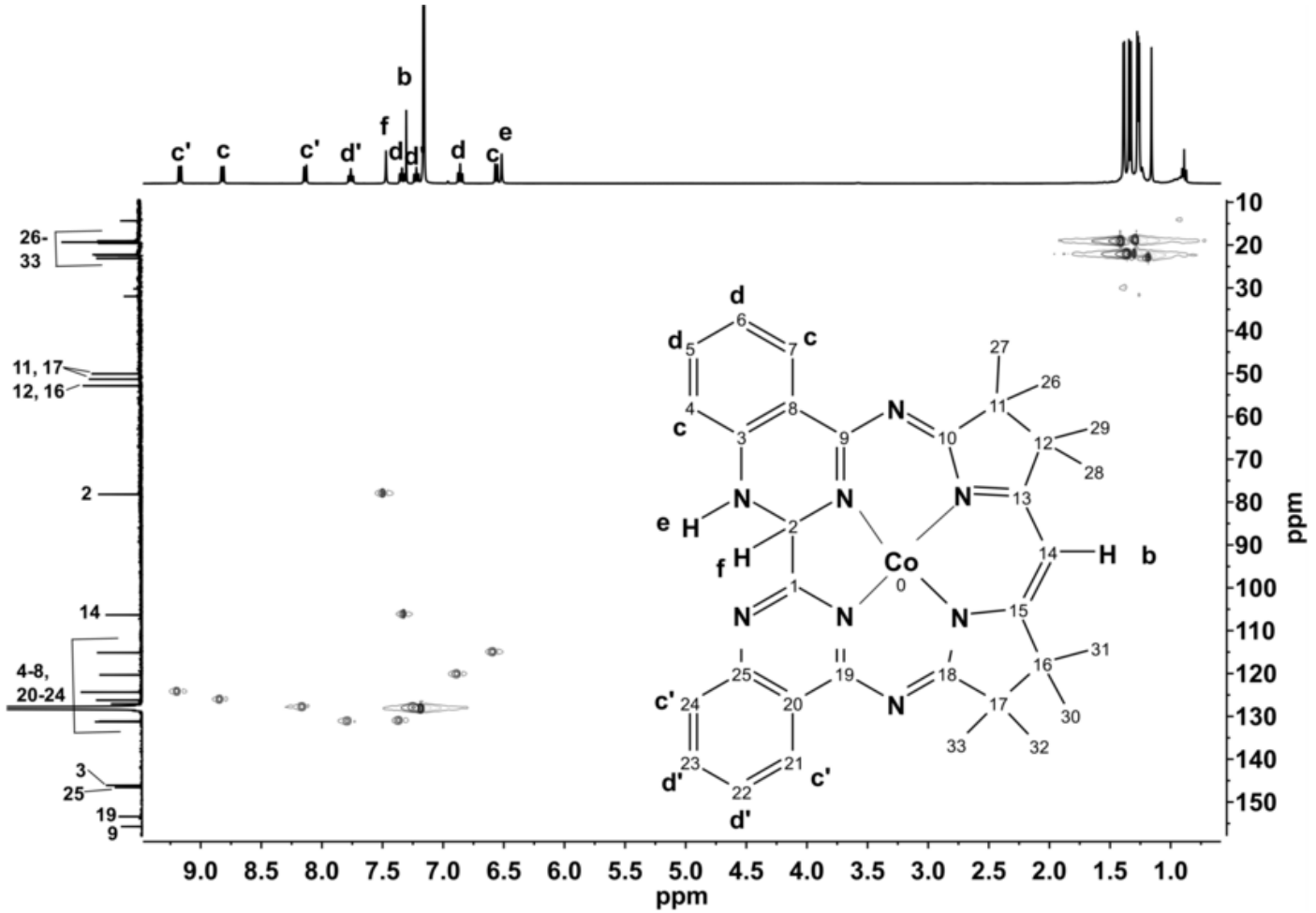

Figure S14. HSQC NMR spectrum of. [**2-H$_2$]** in benzene-d$_6$. The HSQC NMR spectrum of [**2-H$_2$]** shows, that the proton signal at 6.52 ppm (e) is not coupled to a carbon atom, such that the proton can be assigned to an N-H proton. In contrast, the proton resonance at 7.47 ppm (f) can be assigned to a C-bound proton.

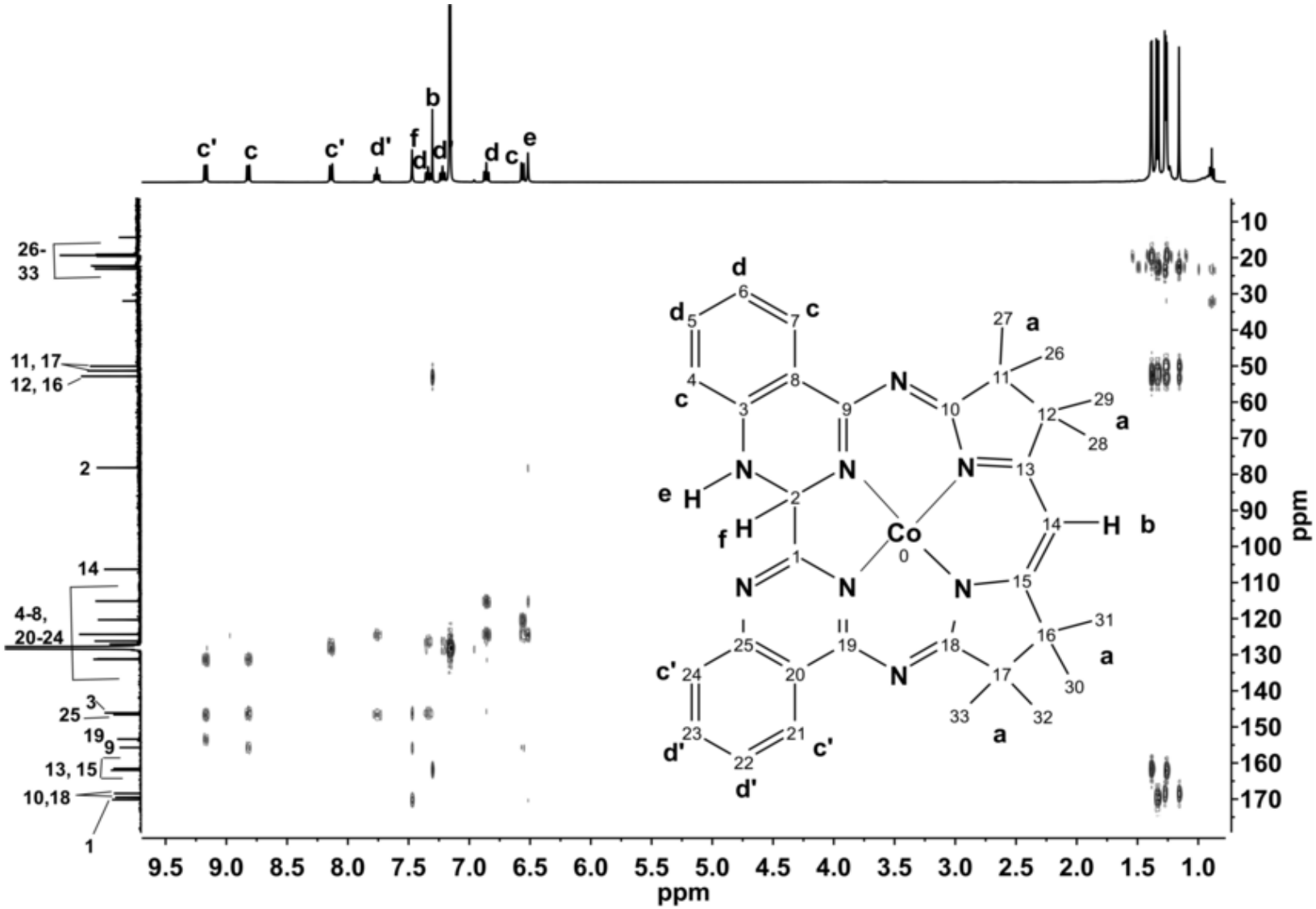
c'
c
c'
d'
f
d
b
d'
d
c
e
26-
33
11, 17
12, 16
2
14
4-8,
20-24
3
25
19
9
13, 15
10,18
1
9.5
9.0
8.5
8.0
7.5
7.0
6.5
6.0
5.5
5.0
4.5
4.0
3.5
3.0
2.5
2.0
1.5
1.0
ppm
10
20
30
40
50
60
70
80
90
100
110
120
130
140
150
160
170
ppm
Co
N
H
a
b
c
c'
d
d'
e
f

Figure S15. HMBC NMR spectrum of. **[2-H_2]** in benzene-d_6.

The proton resonance at 7.30 ppm (b) in the HMBC NMR spectrum of **[2-H_2]** could be assigned to a H atom bound to C14, as only coupling of this resonance to quaternary carbon atoms (C12, 13, 14, 16) is observed. The quaternary carbon atom signals couple to the proton signals of the Mabiq methyl groups, justifying the assignment of the singlet at 7.30 ppm to the diketiminate proton. The proton signal at 7.47 ppm (f) also is coupled solely to quaternary protons, indicating that the proton is attached to C1 or C2. The proton signal at 6.52 ppm (NH, e) is coupled to resonances corresponding to the aromatic C-H atoms and the carbon atom bound to H_f, and is therefore assigned to a proton bound to a bpm nitrogen atom.

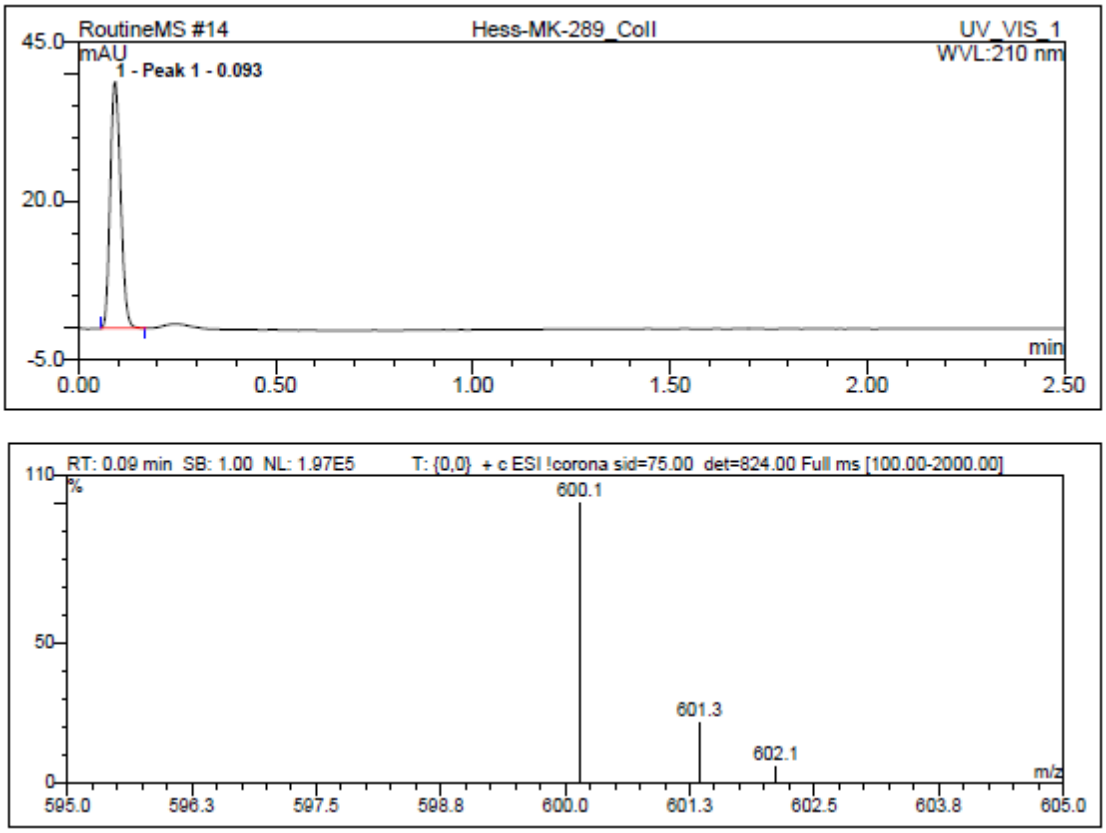

Figure S16. ESI-MS spectrum of **3**.

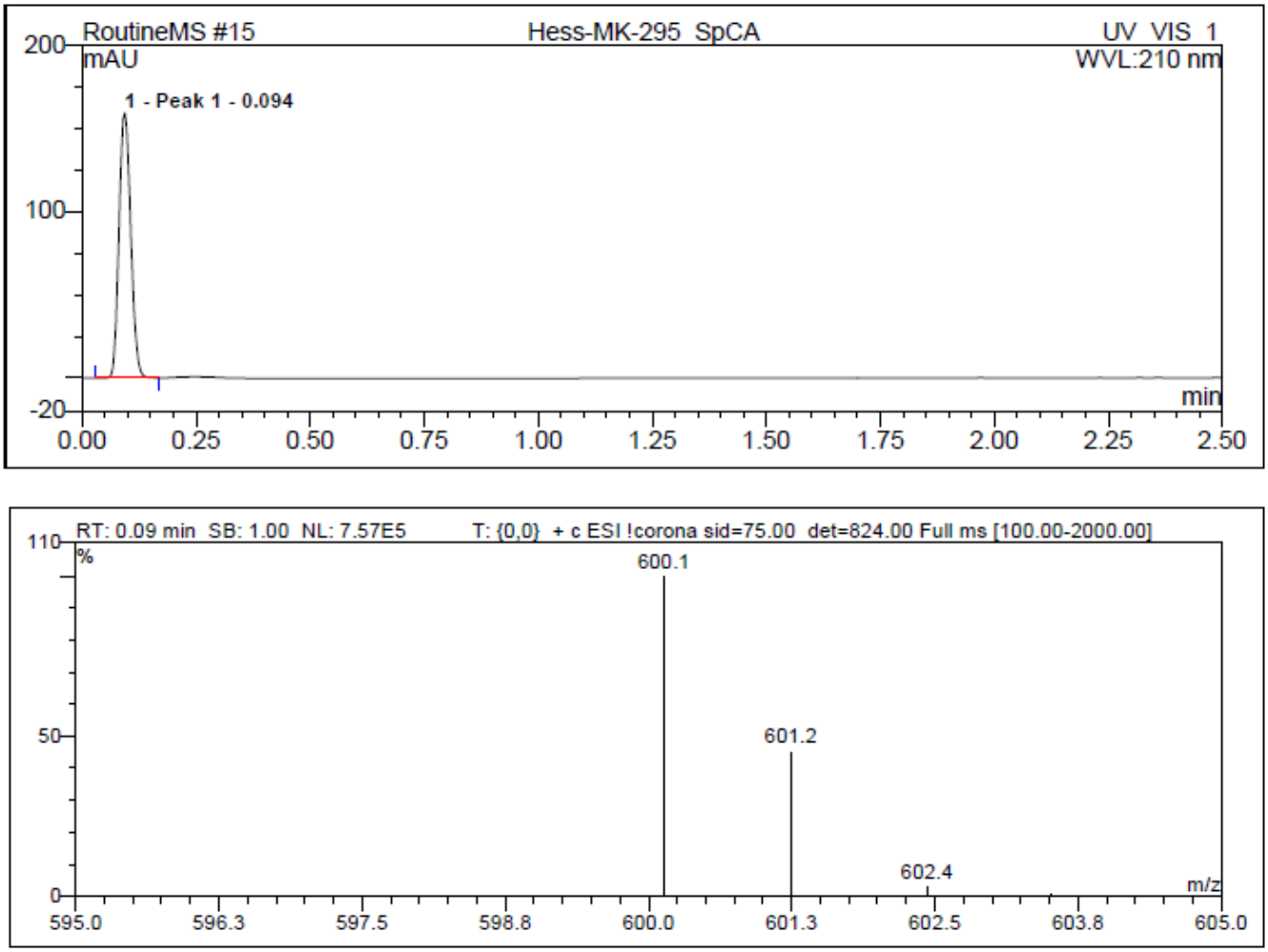

Figure S17. ESI-MS spectrum of a mixture of **3** and 5 equiv. *p*CA.

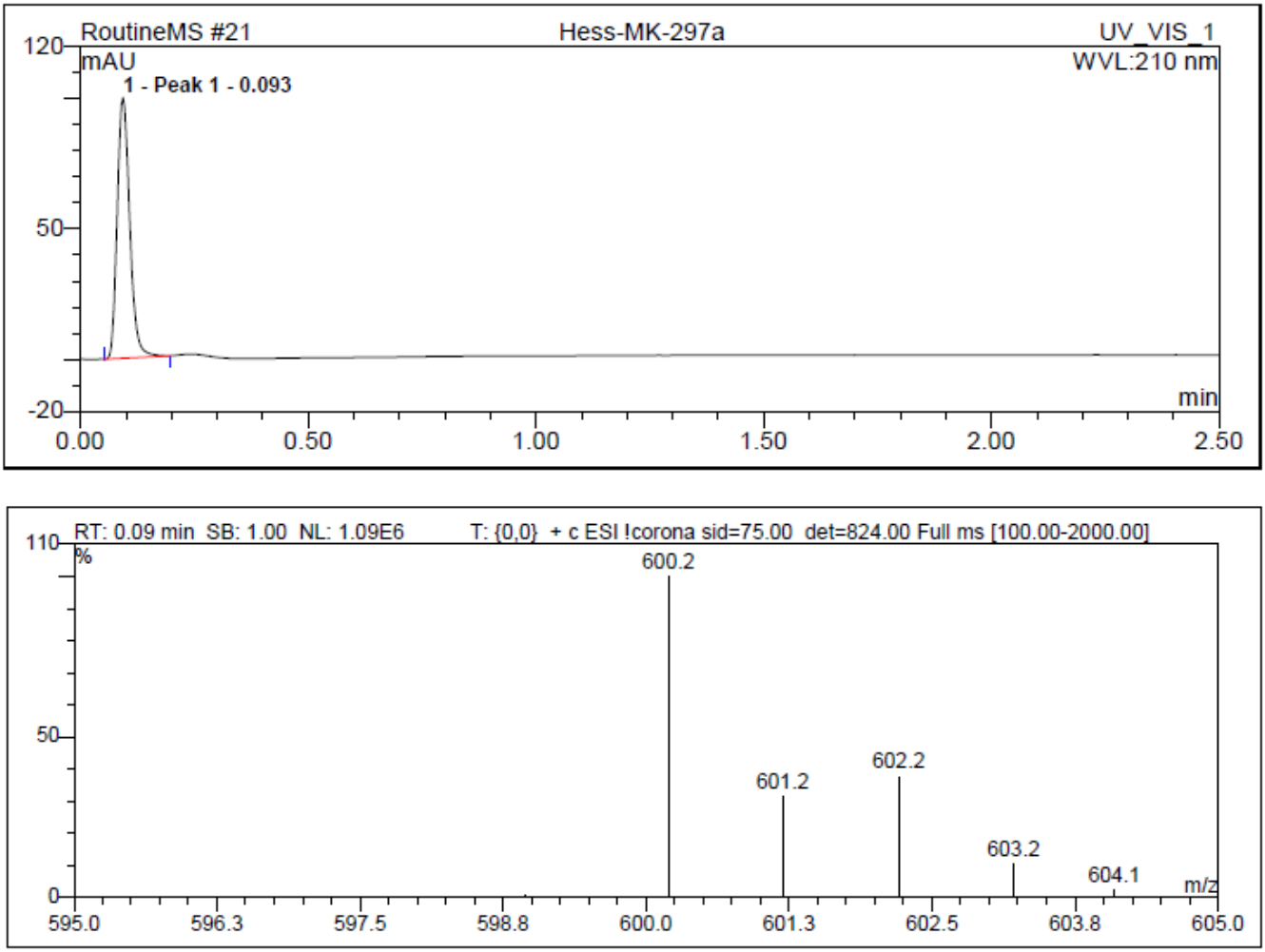

Figure S18. ESI-MS spectrum for the product of **1** plus 1 equiv. *p*CA.

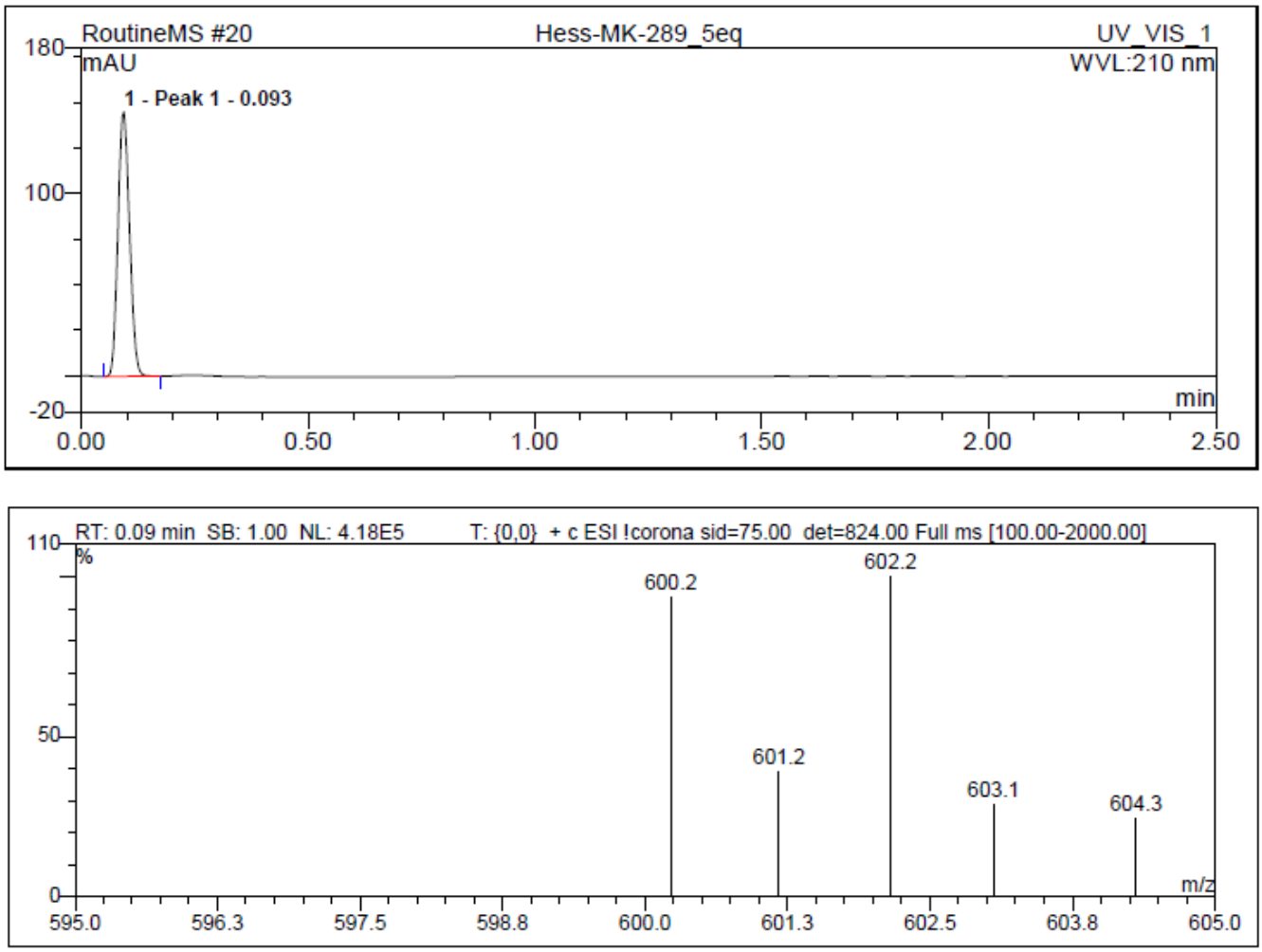

Figure S19. ESI-MS spectrum for the product of **1** plus 5 equiv. *p*CA.

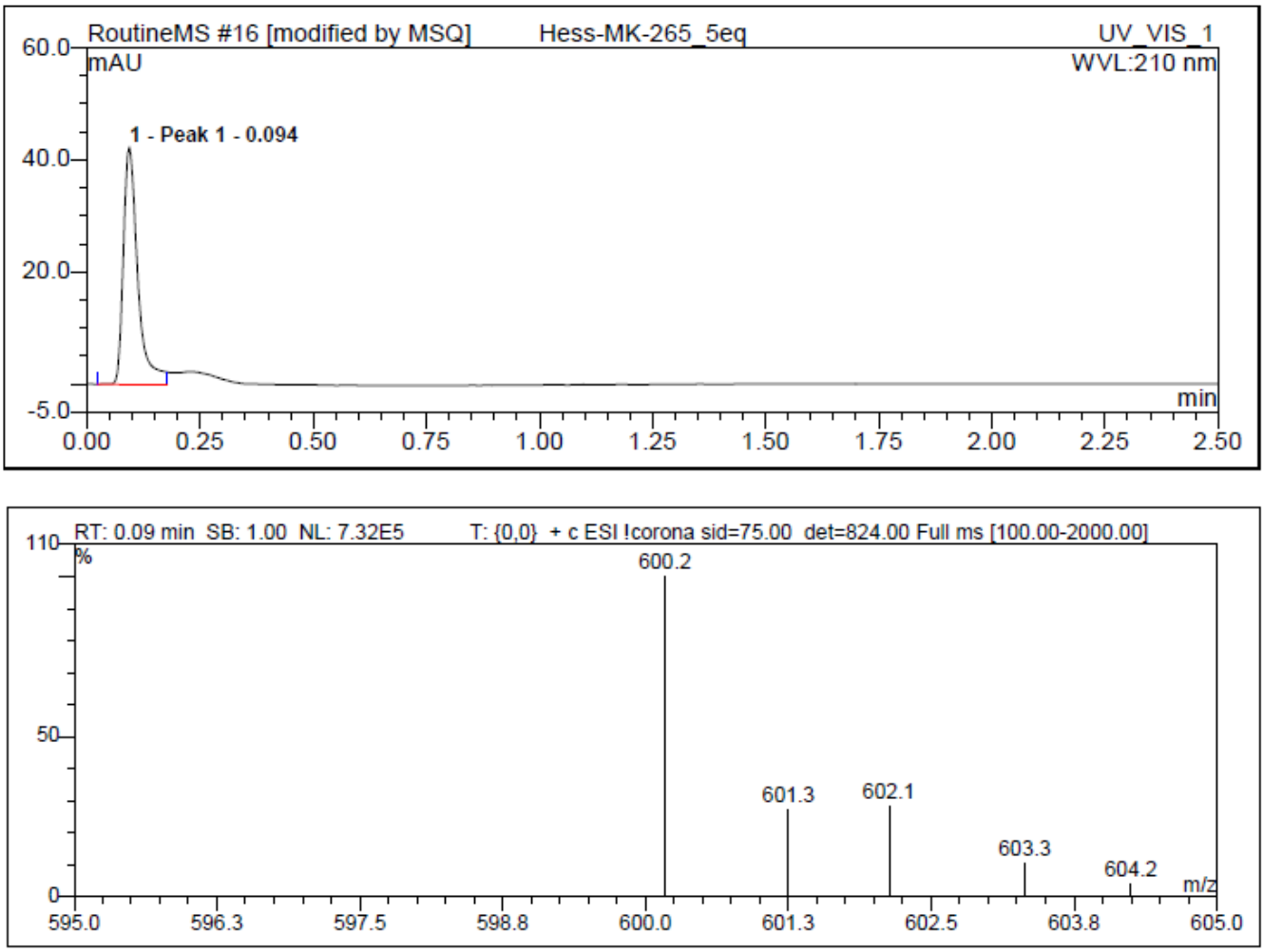

Figure S20. ESI-MS spectrum for the product of **1** plus 5 equiv. benzoic acid.

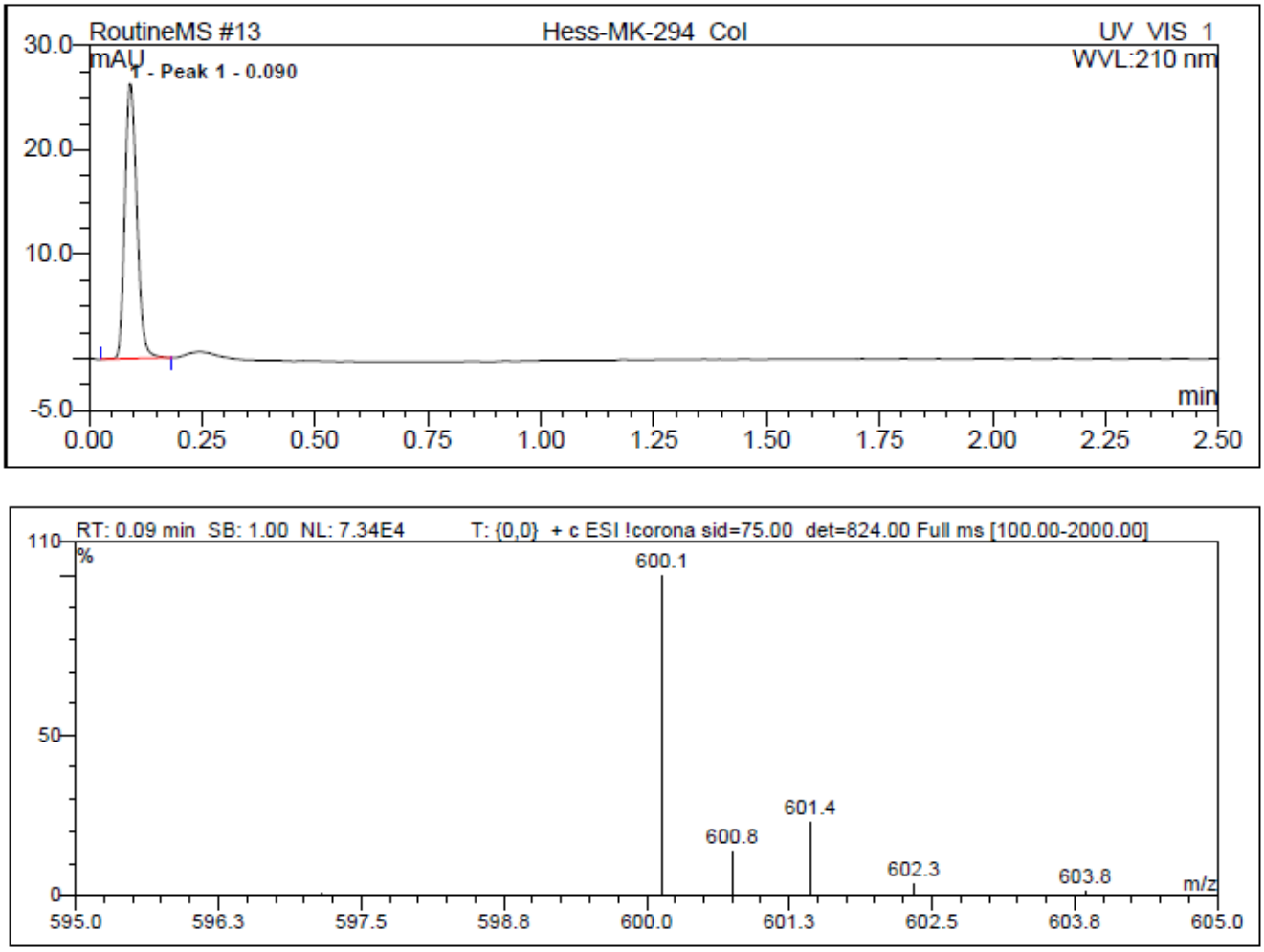

Figure S21. ESI-MS spectrum of **2**.

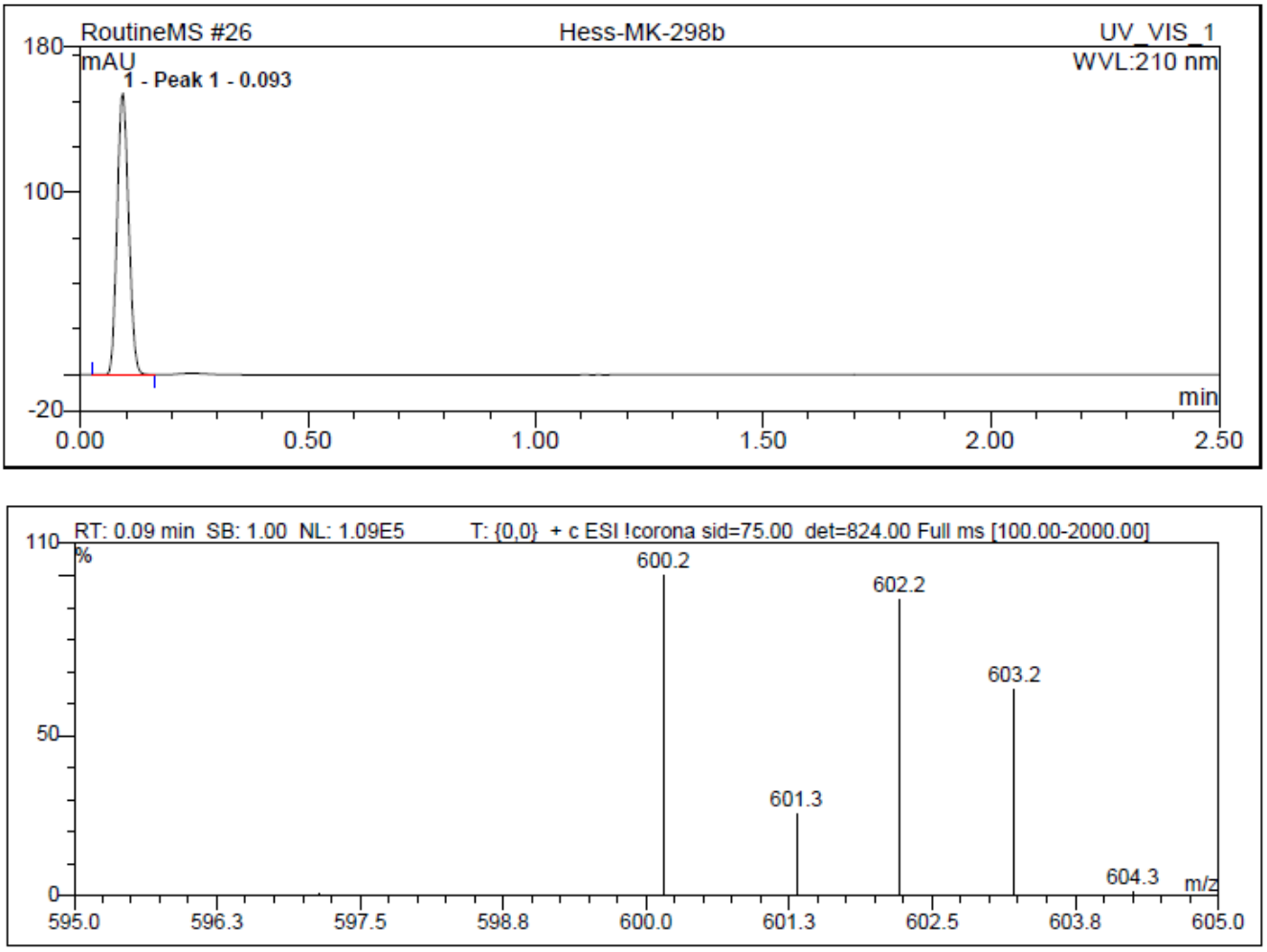

Figure S22. ESI-MS spectrum for the product of **2** plus 5 equiv. *p*CA.

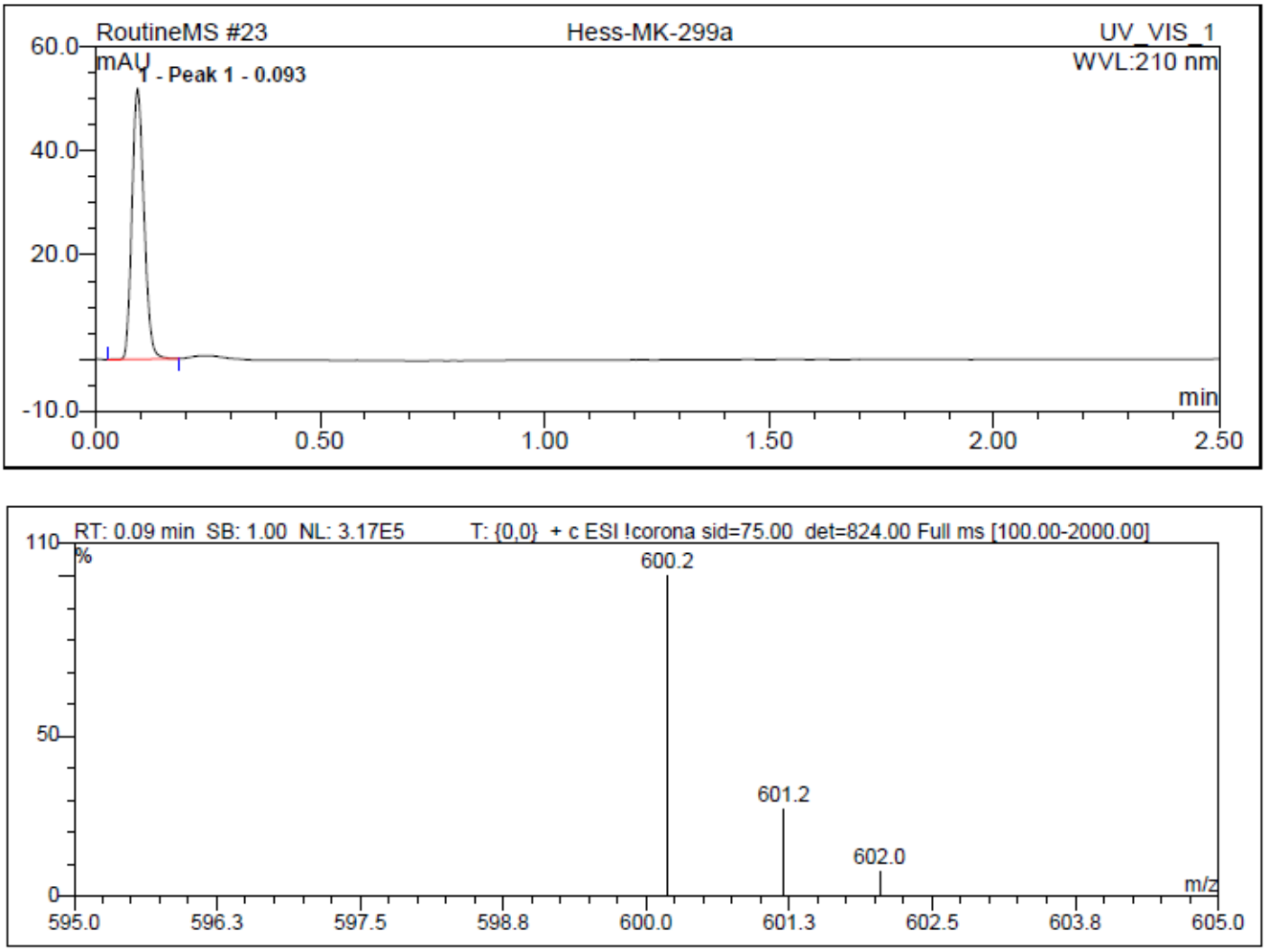

Figure S23. ESI-MS spectrum for the product of **2** plus 5 equiv. benzoic acid.

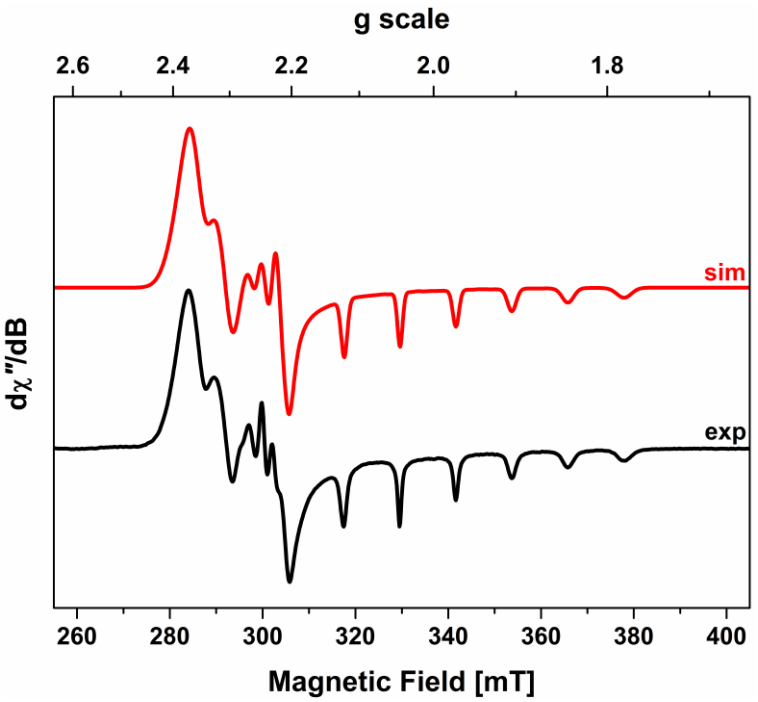

Figure S24. X-band EPR spectrum of **3** recorded in CH_2Cl_2/toluene solution at 130 K (experimental conditions: frequency, 9.4293 GHz; power, 0.63 mW; modulation, 0.3 mT). Experimental data are represented by the black line; simulation is depicted by the red trace: g = (2.285, 2.258, 2.006); $A\{^{59}Co\}$ = (26, 22, 113) × 10^{-4} cm^{-1}; Gaussian linewidths W = (10, 8, 6) × 10^{-4} cm^{-1}; g-strain σ_g = (-0.006, 0.006, 0.0007); A-strain σ_A = (-5, 1, -4).

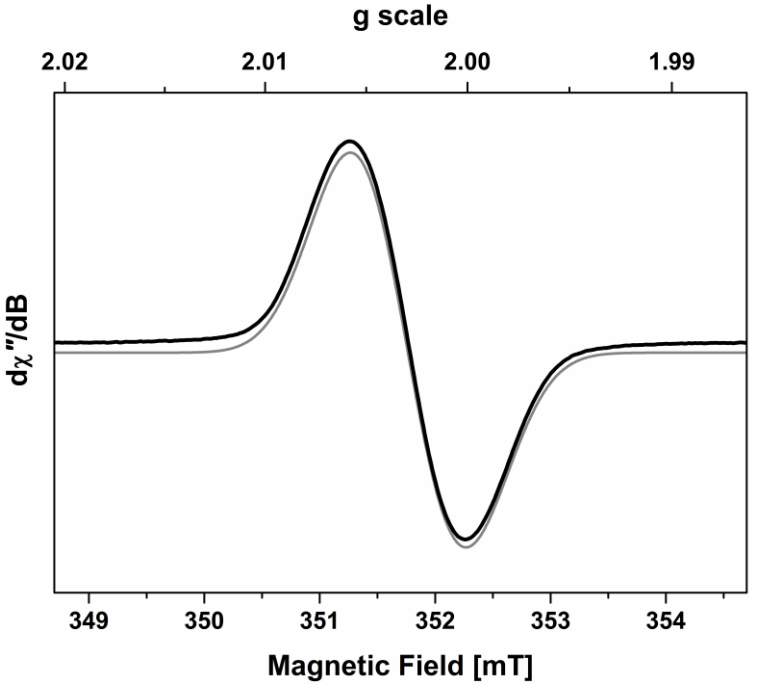

Figure S25. X-band EPR spectrum of **1** recorded in THF solution at 293 K (experimental conditions: frequency, frequency, 9.8612 GHz; power, 0.63 mW; modulation, 0.01 mT). Experimental data are represented by the black line and the simulation by the gray trace: g_{iso} = 2.0029; $A_{iso}\{^{59}Co\}$ = 1.05 × 10^{-4} cm^{-1}; Gaussian linewidth $W = 4.1 \times 10^{-4}$ cm^{-1}.

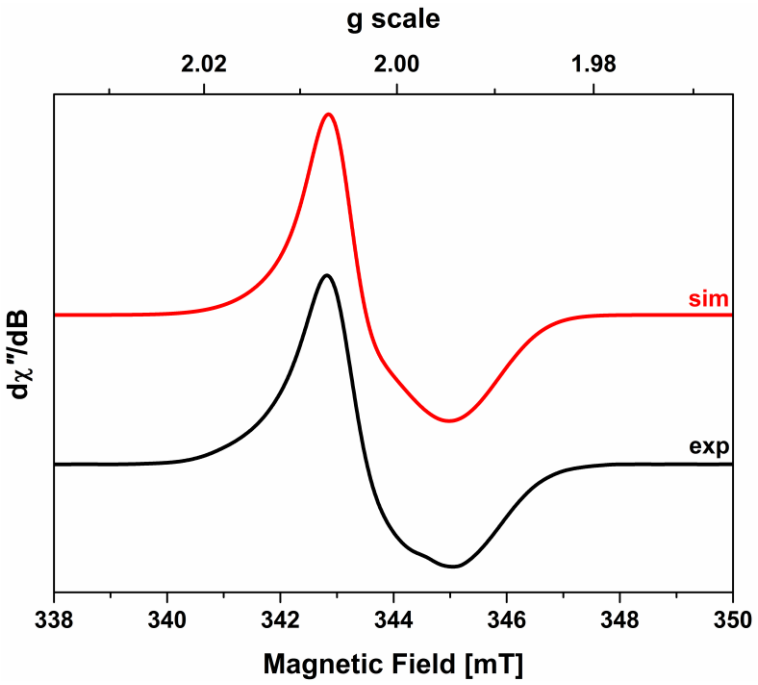

Figure S26. X-band EPR spectrum of **1** recorded in THF solution at 77 K (experimental conditions: frequency, frequency, 9.6311 GHz; power, 2.0 mW; modulation, 0.6 mT). Experimental data are represented by the black line; simulation is depicted by the red trace: g = (2.0056, 2.0042, 1.9941); $A\{^{59}\mathrm{Co}\}$ = (0, 1.5, 1.6) × 10^{-4} cm^{-1}; Gaussian linewidths W = (1.4, 13, 6.5) × 10^{-4} cm^{-1}; g-strain σ_g = (0.0009, 0, 0.0006).

SC-XRD determination of compound [2-H_2]

We performed a single-crystal XRD study on a crystalline specimen of **[2-H_2]**. Although the sample was of small size and limited quality, we were able to obtain a decent model of the structure. The refinement was possible until a stage, where we see strong indications of the addition of H-atoms. However, we were not able to proceed to the point, at which the crystal structure can be presented as a structural proof alone, but together with our results from the NMR experiments, the results from the diffraction experiments are presented as a supporting indication for the hydrogen addition to the ligand.

General crystal data

A dark violet plate-like specimen of $C_{33}H_{35}CoN_8$, approximate dimensions 0.008 mm x 0.115 mm x 0.220 mm, was used for the X-ray crystallographic analysis. The X-ray intensity data were measured on a Bruker D8 Venture system equipped with a Helios optic monochromator and a Mo TXS rotating anode (λ = 0.71073 Å).

The total exposure time was 20.15 hours. The frames were integrated with the Bruker SAINT software package using a narrow-frame algorithm. The integration of the data using an orthorhombic unit cell yielded a total of 82225 reflections to a maximum θ angle of 25.03° (0.84 Å resolution), of which 4932 were independent (average redundancy 16.672, completeness = 99.9%, Rint = 6.94%, Rsig = 2.63%) and 4123 (83.60%) were greater than 2σ(F2). The final cell constants of a = 9.993(2) Å, b = 20.714(5) Å, c = 27.024(6) Å, volume = 5594.(2) Å3, are based upon the refinement of the XYZ-centroids of 153 reflections above 20 σ(I) with 4.776° < 2θ < 41.17°. Data were corrected for absorption effects using the Multi-Scan method (SADABS). The ratio of minimum to maximum apparent transmission was 0.895.

The final anisotropic full-matrix least-squares refinement on F2 with 524 variables converged at R1 = 7.72%, for the observed data and wR2 = 15.18% for all data. The goodness-of-fit was 1.219. The largest peak in the final difference electron density synthesis was 0.466 e-/Å3 and the largest hole was -0.809 e-/Å3 with an RMS deviation of 0.075 e-/Å3. On the basis of the final model, the calculated density was 1.426 g/cm3 and F(000), 2512 e-.

Table S5. Sample and crystal data for **[2-H_2]**.

Identification code	KasMa27	
Chemical formula	$C_{33}H_{35}CoN_8$	
Formula weight	600.60 g/mol	
Temperature	100(2) K	
Wavelength	0.71073 Å	
Crystal size	0.008 x 0.115 x 0.220 mm	
Crystal habit	dark violet plate	
Crystal system	orthorhombic	
Space group	*P b c a*	
Unit cell dimensions	a = 9.993(2) Å	α = 90°
	b = 20.714(5) Å	β = 90°
	c = 27.024(6) Å	γ = 90°
Volume	5594.(2) $Å^3$	
Z	8	
Density (calculated)	1.426 g/cm^3	
Absorption coefficient	0.653 mm^{-1}	
F(000)	2512	
Diffractometer	Bruker D8 Venture	
Radiation source	TXS rotating anode, Mo	
Theta range for data collection	2.38 to 25.03°	
Index ranges	-11<=h<=11, -24<=k<=24, -32<=l<=32	
Reflections collected	82225	
Independent reflections	4932 [R(int) = 0.0694]	
Coverage of independent reflections	99.9%	
Absorption correction	Multi-Scan	
Refinement method	Full-matrix least-squares on F^2	
Refinement program	SHELXL-2014/7 (Sheldrick, 2014)	
Function minimized	$\Sigma w(F_o^2 - F_c^2)^2$	
Data / restraints / parameters	4932 / 188 / 524	
Goodness-of-fit on F^2	1.219	

Table S6. Data collection and structure refinement for **2-H_2**.

Δ/σ_{max}	0.001	
Final R indices	4123 data; $I>2\sigma(I)$	R1 = 0.0772, wR2 = 0.1457
	all data	R1 = 0.0930, wR2 = 0.1518
Weighting scheme	$w=1/[\sigma^2(F_o^2)+(0.0142P)^2+25.6150P]$ where $P=(F_o^2+2F_c^2)/3$	
Largest diff. peak and hole	0.466 and -0.809 eÅ^{-3}	
R.M.S. deviation from mean	0.075 eÅ^{-3}	

Refinement

First, we refined the structure using restraints (SAME, RIGU) for the split-layer positions of the aliphatic groups in the ligand backbone. The resulting intermediate model showed overall prolonged ADPs (Figure S31). Therefore, we also checked for lower symmetries and superstructure reflections, both not yielding improved results.

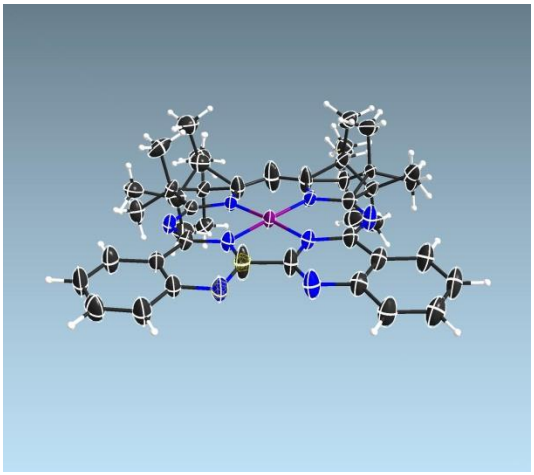

Figure S27. Refined structure of **[2-H_2]** showing prolonged ADPs especially at the bpm-moieties.

The ADPs for the distal nitrogen atoms in the bpm moiety and their adjacent central carbon atoms are significantly more elongated than their neighboring atoms. This is usually a sign for disorder, which is the first indication that the hybridization of these atoms could have be altered from sp^2 (compound **2**) to sp^3 after addition of hydrogen. The next indication for the presence of hydrogen atoms is the existence of positive peaks of residual electron density in close proximity of these elongated ADPs (Figure S32). The peaks are situated on opposite sides of the central complex plane and therefore could likely correspond to hydrogen atoms bound to the central carbon atom and the distal nitrogen atom, respectively.

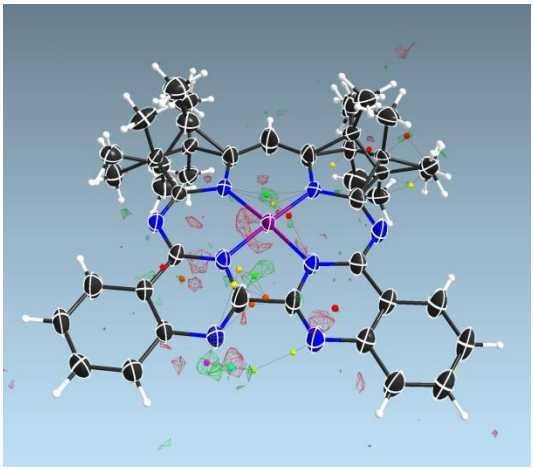

Figure S28. Refined structure of **[2-H$_2$]** showing two peaks in the positive residual electron density at the central atoms of the bpm-moieties. (The residual electron density at the metal atoms is caused by termination effects.)

A split-layer refinement was then performed, modelling a partial occupation of the sp^2-atoms (flat) or the sp^3-atoms, whereafter the two residual electron density peaks are in a meaningful distance to resemble N-H or C-H bonds respectively (Figure S33).

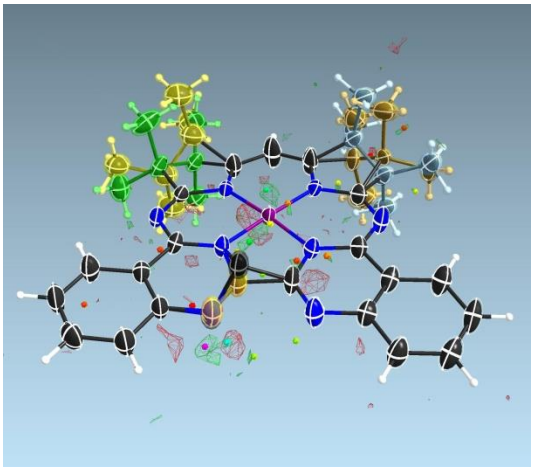

Figure S29. Refined structure of **[2-H$_2$]** showing the split-layer refinements with the two peaks in the positive residual electron density at the central atoms of the bpm-moieties. (The residual electron density at the metal atoms is caused by termination effects.)

This is the best model we were able to refine, since the addition of the protons at the peak positions does not enable the possibility to freely refine them (since their positions are refined towards the neighboring heavier atoms). We refrained from additional restraints to fix the H-positions and to model the same effect on the opposing side of the ligand, since the indications are already visible. Therefore, the SC-XRD determination strongly indicates, that the observed existence of additional H-atoms in the solution NMR-experiments can also be observed in the solid state.

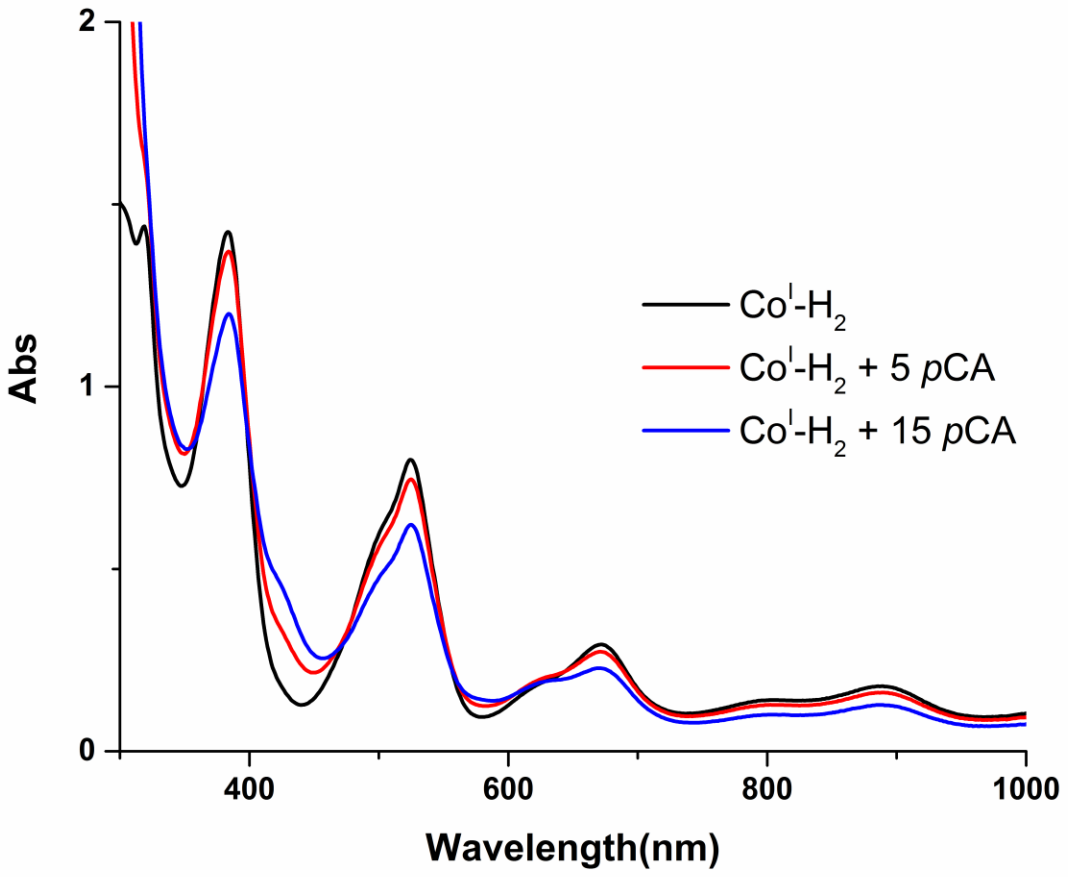

Figure S30. Electronic spectra of the reaction products of **[2-H$_2$]** with *p*CA.

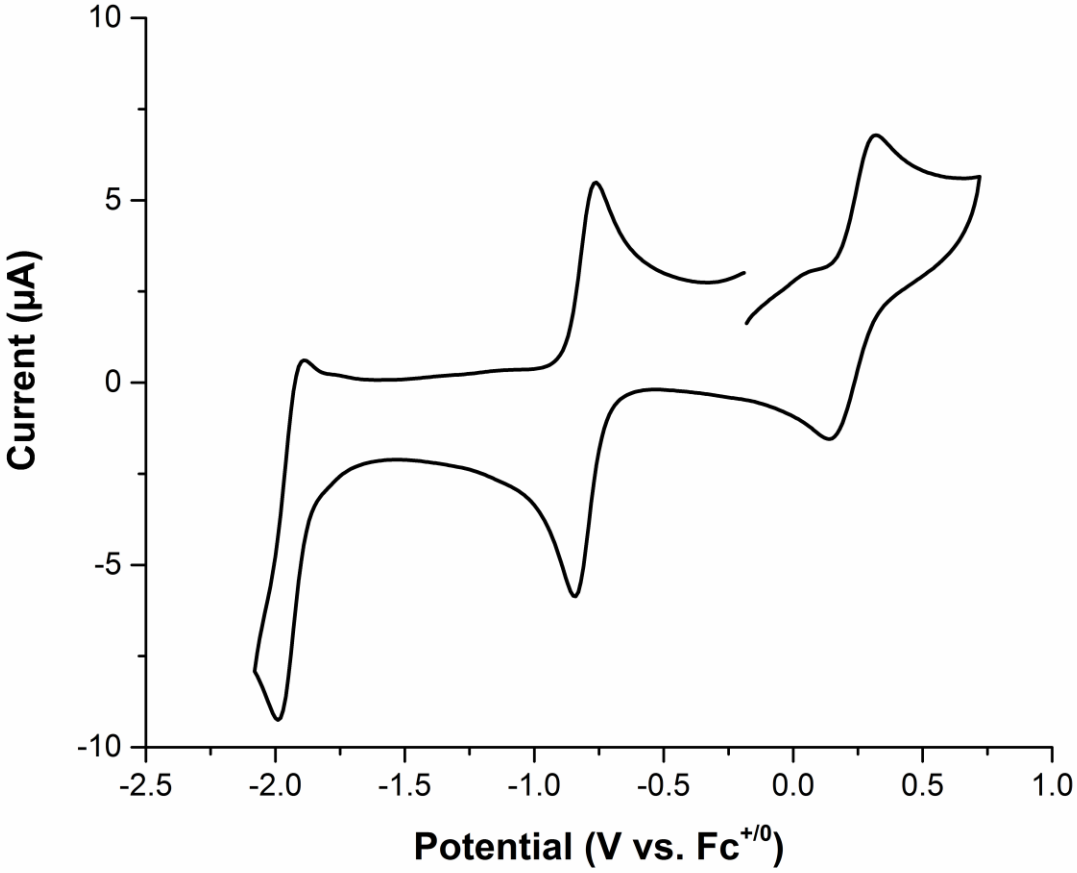

Fig. S31. Cyclic voltammogram of **[2-H_2]** (1.0 mM) in MeCN; 0.1 M [N(*n*-Bu)$_4$]PF_6; scan rate: 0.1 V/s.

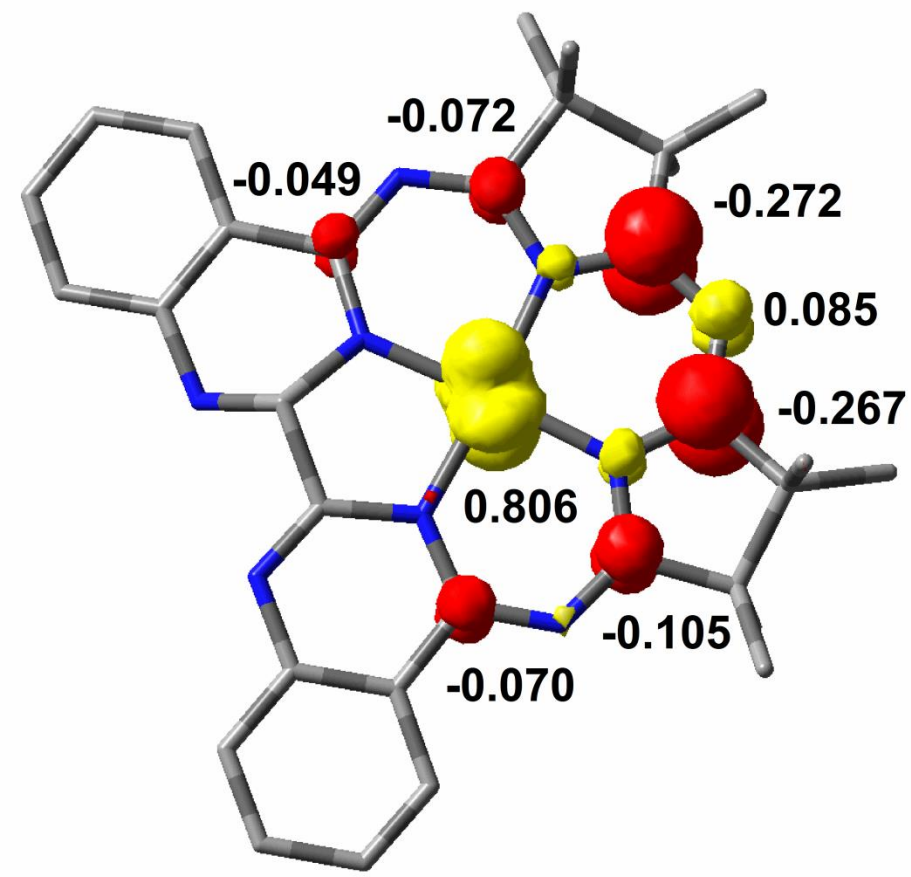

Fig. S32. DFT-derived (B3LYP) spin density plot for **[2-H_2]** based on Löwdin population analysis.

References

[1] D. Coucouvanis, *Useful Reagents and Ligands* in *Inorganic Syntheses, Vol. 33*, John Wiley & Sons, Inc., New York, **2002,** pp. 75-121.
[2] A. M. Appel, D. L. DuBois, M. Rakowski DuBois, *Journal of the American Chemical Society* **2005**, *127*, 12717.
[3] E. Müller, G. Bernardinelli, A. von Zelewsky, *Inorg. Chem.* **1988**, *27*, 4645.
[4] P. Banerjee, A. Company, T. Weyhermüller, E. Bill, C. R. Hess, *Inorg. Chem.* **2009**, *48*, 2944.
[5] E. V. Puttock, P. Banerjee, M. Kaspar, L. Drennen, D. S. Yufit, E. Bill, S. Sproules, C. R. Hess, *Inorganic Chemistry* **2015**, *54*, 5864.
[6] G. R. Hanson, K. E. Gates, C. J. Noble, M. Griffin, A. Mitchell, S. Benson, *J. Inorg. Biochem.* **2004**, *98*, 903.
[7] *APEX suite of crystallographic software, APEX 2, version 2008.4.*, Bruker AXS Inc.
[8] *SAINT, version 7.56a, SADABS, version 2008.1*, Bruker AXS Inc.
[9] C. B. Hübschle, G. M. Sheldrick, B. Dittrich, *SHELXLE, J. Appl. Crystallogr.* **2011**, *44*, 1281.
[10] G. M. Sheldrick, *SHELXL-2014*, University of Göttingen.
[11] G. M. Sheldrick, *SHELXL-97*, University of Göttingen.
[12] A. J. C. Wilson, *International Tables for Crystallography*, Dordrecht.
[13] A. L. Spek, *J. Appl. Cryst.* **2003**, *36*, 7.
[14] A. L. Spek, *Acta Cryst.* **2009**, *D65*, 148.
[15] A. L. Spek, *Acta Cryst.* **2015**, *C71*, 9.
[16] F. Neese, Version 3.0.3 ed., Max Plank Institute for Bioinorganic Chemistry, Mühlheim an der Ruhr, Germany, **Jan 2012**.
[17] A. D. Becke, *J. Chem. Phys.* **1986**, *84*, 4524.
[18] A. D. Becke, *J. Chem. Phys.* **1993**, *98*, 5648.
[19] C. T. Lee, W. T. Yang, R. G. Parr, *Phys. Rev. B* **1988**, *37*, 785.
[20] A. Schäfer, H. Horn, R. Ahlrichs, *J. Chem. Phys.* **1992**, *97*, 2571.
[21] A. Schäfer, C. Huber, R. Ahlrichs, *J. Chem. Phys.* **1994**, *100*, 5829.
[22] K. Eichkorn, O. Treutler, H. Ohm, M. Häser, R. Ahlrichs, *Chem. Phys. Lett.* **1995**, *240*, 283.
[23] K. Eichkorn, O. Treutler, H. Ohm, M. Häser, R. Ahlrichs, *Chem. Phys. Lett.* **1995**, *242*, 652.
[24] R. Dennington, T. Keith, J. Milliam, Version 5.0 ed., Semichem Inc., Shawnee Mission KS, **2009**.
[25] D. H. Pool, M. P. Stewart, M. O'Hagan, W. J. Shaw, J. A. S. Roberts, R. M. Bullock, D. L. DuBois, *Proc. Natl. Acad. Sci.* **2012**, *109*, 15634.